

Numerical solution of Riemann–Hilbert problems: random matrix theory and orthogonal polynomials

Sheehan Olver and Thomas Trogdon

October 30, 2018

Abstract

In recent developments, a general approach for solving Riemann–Hilbert problems numerically has been developed. We review this numerical framework, and apply it to the calculation of orthogonal polynomials on the real line. Combining this numerical algorithm with an approach to compute Fredholm determinants, we are able to calculate level densities and gap statistics for general finite-dimensional unitary ensembles. We also include a description of how to compute the Hastings–McLeod solution of the homogeneous Painlevé II equation.

1 Introduction

We are concerned with calculating random matrix statistics for Hermitian invariant ensembles; i.e., $n \times n$ random matrices

$$M = \begin{pmatrix} M_{11} & M_{12}^R + iM_{12}^I & \cdots & M_{1n}^R + iM_{1n}^I \\ M_{12}^R - iM_{12}^I & M_{22} & \cdots & M_{2n}^R + iM_{2n}^I \\ \vdots & \ddots & \ddots & \vdots \\ M_{1n}^R - iM_{1n}^I & \cdots & M_{(n-1)n}^R - iM_{(n-1)n}^I & M_{nn} \end{pmatrix}$$

whose entries are distributed according to

$$\frac{1}{Z_n} e^{-n \operatorname{Tr} V(M)} dM,$$

where Z_n is the normalization constant and

$$dM = \prod_{i=1}^n dM_{ii} \prod_{i < j} (dM_{ij}^R dM_{ij}^I).$$

The eigenvalue statistics of invariant ensembles are expressible in terms of the kernel

$$\mathcal{K}_n(x, y) = -\frac{\gamma_{n-1} e^{-n/2(V(x)+V(y))}}{2\pi i} \frac{\pi_n(x)\pi_{n-1}(y) - \pi_{n-1}(x)\pi_n(y)}{x - y}, \quad [6]$$

where π_k are the orthonormal polynomials π_0, π_1, \dots with respect to the weight

$$e^{-nV(x)} dx,$$

and

$$\gamma_{n-1} = 2\pi i \left[\int_{-1}^1 \pi_{n-1}(x)w(x) dx \right]^{-1}$$

is a normalization constant. Particular statistics include the *level density*

$$d\mu_n = \mathcal{K}_n(x, x) dx,$$

describing the global distribution of eigenvalues, and the *gap statistic*

$$\det(I - \mathcal{K}_n|_{L^2[\Omega]}),$$

where \det denotes a *Fredholm determinant*, describing the local distribution of eigenvalues; namely, the probability that no eigenvalue is inside the set Ω .

Gap statistics for invariant ensembles follow two principles of universality. For x in the *bulk* — i.e., inside the support of the equilibrium measure — the gap statistic of a properly scaled neighbourhood of x will approach the sinc kernel distribution:

$$\det(I - \mathcal{S}|_{L^2(-s,s)}) \quad \text{for} \quad \mathcal{S} = \frac{\sin(x-y)}{x-y}.$$

This was proved rigorously in [6] by expressing the orthogonal polynomials in terms of a *Riemann–Hilbert problem*, so that asymptotics of π_n were determinable via nonlinear steepest descent. Moreover, the *edge statistic* — i.e., a properly scaled neighbourhood of ∞ — generically approaches the Tracy–Widom distribution:

$$\det(I - \mathcal{A}|_{L^2(s,\infty)}) \quad \text{for} \quad \mathcal{A} = \frac{\text{Ai}(x)\text{Ai}'(y) - \text{Ai}'(x)\text{Ai}(y)}{x-y}.$$

Underlying these two universality laws are *Painlevé transcendents*; in the case of the Tracy–Widom distribution it is the Hastings–McLeod solution to Painlevé II [16], whereas the sine kernel distribution is expressible in terms of a solution to Painlevé V [17]. See Section A for a discussion of a numerical Riemann–Hilbert approach for computing the Hastings–McLeod solution of Painlevé II.

The statistics differ from universality laws for finite n and are no longer expressible in terms of Painlevé transcendents. Hence our aim is to calculate the finite-dimensional statistics to explore the manner in which the onset of universality depends on the potential V . To accomplish this task, we will calculate the associated orthogonal polynomials numerically, also using their Riemann–Hilbert representation, via the framework of [21, 22]. By deforming the contours appropriately, we will achieve a numerical method that is uniformly accurate for large and small n , as shown in [23].

We will see in our numerical experiments that the onset of universality depends strongly on the magnitude of the equilibrium measure: where eigenvalue density is small, finite n statistics differ from universality behaviour greatly.

We begin with a demonstration of the numerically calculated finite-dimensional random matrix statistics (Section 2). Importantly, because we do not require the knowledge of local parametrices, our numerical approach continues to work for degenerate potentials, such as those that arise in the study of higher order Tracy–Widom distributions [4]. We describe the manner in which orthogonal polynomials can be reduced to a Riemann–Hilbert problem that is suitable for numerics (Section 3). We then review the numerical method for Riemann–Hilbert problems (Section 4), based on the deformations of [6]. This includes the result that the numerical approximation is *uniformly accurate* when the contours are appropriately deformed (Section 5), without the use of classical local parametrices.

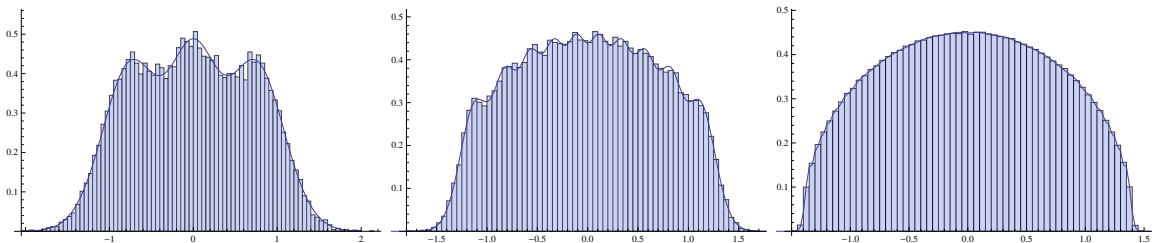


Figure 1: Calculated level densities for the GUE for $n = 3, 10$ and 100 , compared to histograms.

Remark An alternative to the approach advocated in this paper is to calculate the orthogonal polynomials directly for each n via Gram–Schmidt and numerical quadrature. For small n , this is likely to be more efficient. However, it is well known to be prone to instability [15]; moreover, the calculation must be restarted for each n as the weight e^{-nV} changes. On the other hand, the RH approach has computational cost independent of n , making it more practical for investigating large n behaviour.

2 Random matrix theory

Recall that

$$\mathcal{K}_n(x, y) = -\frac{\gamma_{n-1}e^{-n/2(V(x)+V(y))}}{2\pi i} \frac{\pi_n(x)\pi_{n-1}(y) - \pi_{n-1}(x)\pi_n(y)}{x - y}$$

and

$$\mathcal{K}_n(x, x) = -\frac{\gamma_{n-1}e^{-nV(x)}}{2\pi i} (\pi'_n(x)\pi_{n-1}(x) - \pi'_{n-1}(x)\pi_n(x)).$$

In this section, we use the approach of numerically calculating π_n and $\gamma_{n-1}\pi_{n-1}$ that we develop below to compute the finite n statistics. What will be apparent in the numerical results is that the behaviour of local statistics is tied strongly to the global density of eigenvalues near the region; i.e., the magnitude of the level density.

For unitary invariant ensembles, the level density is the distribution of the counting measure. This is precisely

$$d\mu_n = \frac{\mathcal{K}_n(x, x)}{n} dx.$$

In Figure 1, we compare the (numerically calculated) GUE (i.e., $V(x) = x^2$) level density for $n = 3, 10$ and 100 to a histogram, demonstrating the accuracy of the approximation. (Because the polynomials involved are Hermite polynomials, we can also verify the accuracy directly.) This shows the standard phenomena that the distribution exhibits n “bumps” of increased density, corresponding to the positions of the finite charge energy minimization equilibrium; i.e., the Fekete points.

In Figure 2, we plot the finite n level densities for the potential

$$V(x) = \frac{x^2}{5} - \frac{4}{15}x^3 + \frac{x^4}{20} + \frac{8}{5}x,$$

which is an example of a potential whose equilibrium measure vanishes at an endpoint, and hence the edge statistics follow the higher order Tracy–Widom distribution [4]. Interestingly, this change in edge statistic behaviour is not just present in the local statistics, but clearly visible in the decay of the tail of the global statistics.

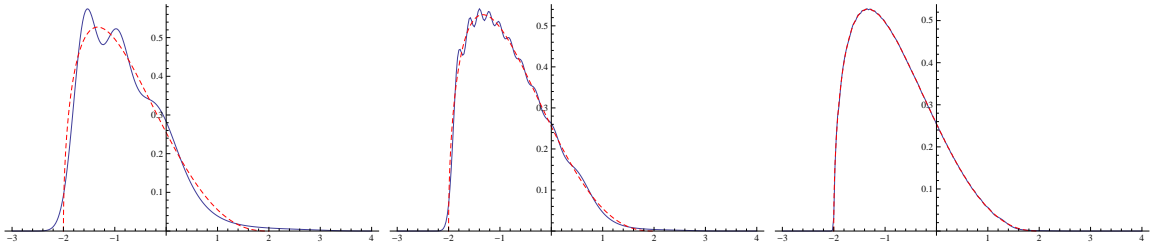


Figure 2: Calculated level density for $V(x) = \frac{x^2}{5} - \frac{4}{15}x^3 + \frac{x^4}{20} + \frac{8}{5}x$ for $n = 3, 10$ and 100 . Dashed line is the equilibrium measure ($n = \infty$).

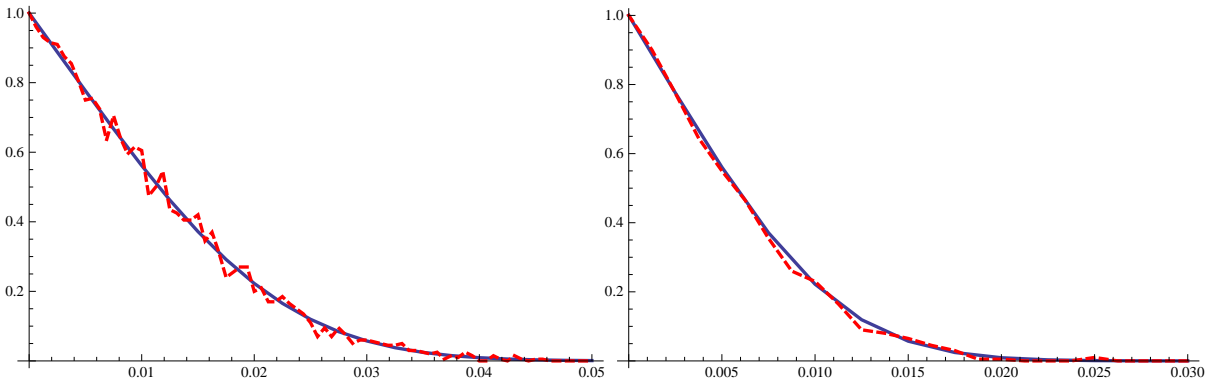


Figure 3: The calculated probability that there are no eigenvalues in $(-s, s)$ for the GUE (plain) versus Monte Carlo simulation (dashed), for $n = 50$ (left) and $n = 100$ (right).

We now turn our attention to local gap statistics, which are described by the *Fredholm determinant*

$$\det(I - \mathcal{K}_n|_{L^2[\Omega]}).$$

Using the method of Bornemann [3], we can calculate the determinant, provided that the kernel itself can be evaluated. Thus, we can successfully calculate finite gap statistics by using the RH approach to calculate π_n and $\gamma_{n-1}\pi_{n-1}$. In Figure 3, we plot the gap statistics versus a histogram for the GUE in the interval $(-s, s)$.

To see universality in the bulk, we have to scale the interval with n ; in particular, we need to look at the gap probability for

$$\Omega = x + \frac{(-s, s)}{\mathcal{K}_n(x, x)}.$$

Alternatively, $\mathcal{K}_n(x, x)$ can be replaced by its asymptotic distribution to get

$$\Omega = x + \frac{(-s, s)}{n\psi(x)},$$

where $d\mu = \psi(x) dx$ is the equilibrium measure of V . For x inside the support of μ , this statistic approaches the sine kernel distribution. We demonstrate this in Figure 4 for the degenerate potential, showing that the rate in which the statistics approach universality depends on the magnitude of the equilibrium measure.

We now turn our attention to edge statistics. In the generic position (i.e., when the equilibrium measure has precisely square root decay at its right endpoint), the gap probability for

$$\Omega = \left(b + \frac{s}{cn^{2/3}}, \infty\right)$$

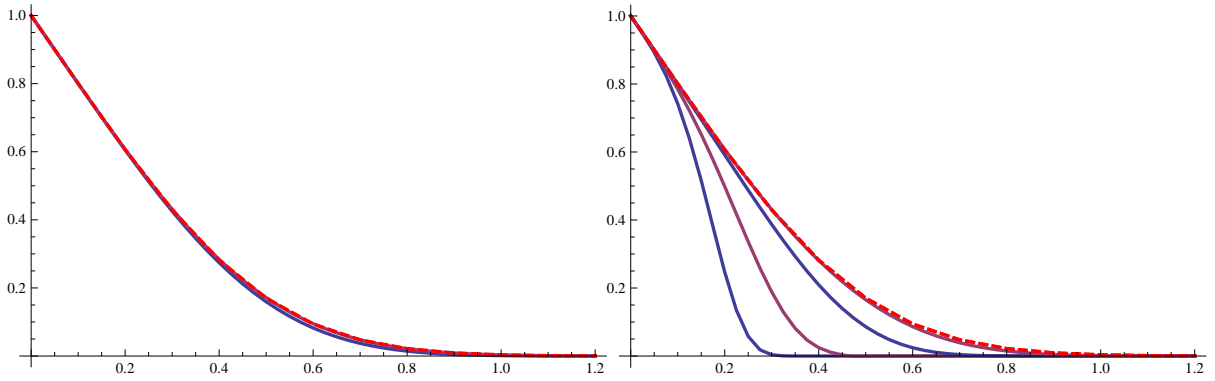


Figure 4: The calculated probability that there are no eigenvalues in the scaled neighbourhood $x + \frac{(-s,s)}{\mathcal{K}_n(x,x)}$ for $n = 50, 100, 200$ and 250 for $x = 1$ (left) and $x = 1.5$ (right), for the potential $V(x) = \frac{x^2}{5} - \frac{4}{15}x^3 + \frac{x^4}{20} + \frac{8}{5}x$.

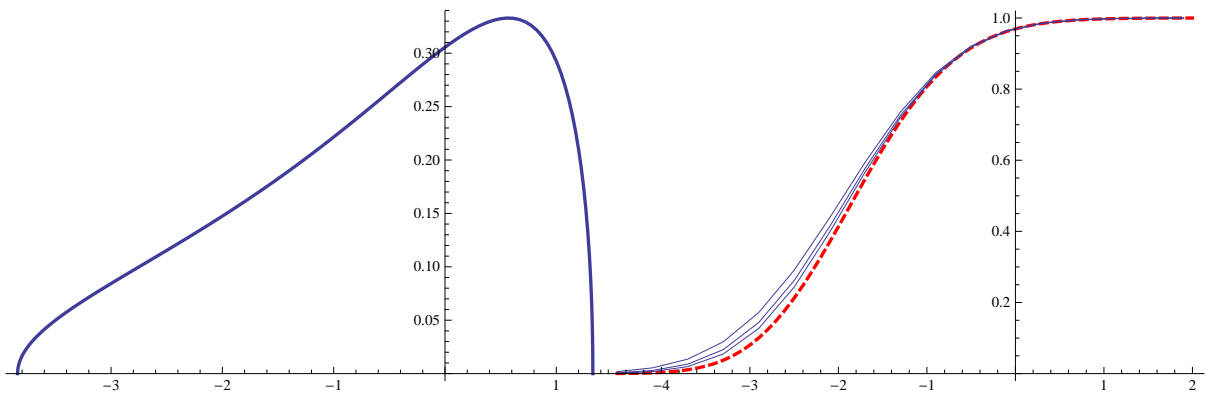


Figure 5: The equilibrium measure for $V(x) = e^x - x$ (left) and the scaled gap statistic for $n = 10, 20, 40$ and 80 (right). The dashed line is the Tracy–Widom distribution ($n = \infty$).

tends to the Tracy–Widom distribution; here c is a constant associated with the equilibrium measure, see Section 3.2 for its precise definition and the numerical method for its calculation. In Figure 5, we plot the computed equilibrium measure for $V(x) = e^x - x$ (computed as described in Section 3.1), and its scaled edge statistic for increasing values of n . While the finite statistics are clearly converging to the Tracy–Widom distribution, the rate of convergence is much slower than the convergence of bulk statistics where the density of the equilibrium measure is large.

Remark There are several methods for calculating universality laws — i.e., $n = \infty$ statistics — including using their Painlevé transcendent representations, see [2] for an overview. An additional approach based on RH problems is to represent, say,

$$\partial_s \log \det(I - \mathcal{S}|_{L^2(-s,s)})$$

as a RH problem. This can be solved numerically for multiple choices of s , and the results integrated numerically, see [5] for examples in the degenerate case. This will be accurate in the tails, whereas the Fredholm determinant representation that we use only achieves absolute accuracy. However, we are not aware of similar RH problems for finite n .

3 Orthogonal polynomials

We wish to calculate the monic polynomials $\pi_0(x), \pi_1(x), \dots$ with respect to the measure

$$e^{-nV(x)} dx$$

supported on the real line. Consider the following RH problem:

Problem 1 [13] *The function*

$$Y(z) = \begin{pmatrix} \pi_n(z) & \mathcal{C}[\pi_n e^{-nV}](z) \\ \gamma_{n-1} \pi_{n-1}(z) & \gamma_{n-1} \mathcal{C}[\pi_{n-1} e^{-nV}](z) \end{pmatrix}$$

where

$$\gamma_{n-1} = 2\pi i \left[\int_{-1}^1 \pi_{n-1}(x) w(x) dx \right]^{-1}$$

solves the RH problem

$$Y_+ = Y_- \begin{pmatrix} 1 & e^{-nV(x)} \\ & 1 \end{pmatrix} \quad \text{and} \quad Y \sim \begin{pmatrix} z^n & \\ & z^{-n} \end{pmatrix}$$

To apply the numerical method described in Section 4, we must transform the RH problem for Y into a suitable form for numerical solution. To accomplish this, we will transform Y by representing it explicitly in terms of new functions which satisfy the following properties:

1. $Y \mapsto T$ so that $T \sim I$ at infinity.
2. $T \mapsto S$ so that the oscillatory jumps of T become exponential decaying jumps of S .
3. $S \mapsto \Phi$ so that the jumps of Φ are localized and scaled.

3.1 Equilibrium measures

Our first task is to remove the growth in Y at ∞ . To accomplish this, we must compute a so-called g -function associated with the equilibrium measure of V :

Definition 1 *The equilibrium measure μ is the minimizer of*

$$\iint \log \frac{1}{|x-y|} d\mu(x) d\mu(y) + \int V(x) d\mu(x).$$

In this section, we assume that the equilibrium measure of V is supported on a single interval (a, b) ; a sufficient condition is that V is convex [6]. (We remark that the below procedure was adapted to the multiple interval case in [19], and adapting our numerical procedure for computing orthogonal polynomials, and thence invariant ensemble statistics, to such cases would be straightforward.)

With the correct choice of (a, b) , there exists g analytic off (a, b) satisfying

$$g_+(x) + g_-(x) = V(x) - \ell \quad \text{for } a \leq x \leq b \quad \text{and} \quad g(z) \sim \log z.$$

The derivative $\phi = g'$ is analytic off (a, b) and satisfies

$$\phi_+(x) + \phi_-(x) = V'(x) \quad \text{for } a \leq x \leq b \quad \text{and} \quad \phi(z) \sim \frac{1}{z}.$$

Given a candidate (a, b) , we can describe all ϕ satisfying this property

Theorem 1 [19] Denote the affine map from (a, b) to $(-1, 1)$ as

$$M_{(a,b)}(z) = \frac{2z - a - b}{b - a}.$$

Suppose we have

$$V'(M_{(a,b)}^{-1}(x)) = \sum_{k=0}^{\infty} V_k T_k(x),$$

where T_k is the k th order Chebyshev polynomial of the second kind. If

$$\phi_+(x) + \phi_-(x) = V'(x) \quad \text{for } x \in (a, b) \quad \text{and} \quad \phi(\infty) = 0,$$

then there exists a χ such that

$$\phi(z) = \sum_{k=0}^{\infty} V_k J_+^{-1}(M_{(a,b)}(z))^k - \frac{V_k}{2} M_{(a,b)}(z) \frac{b-a}{2\sqrt{z-b}\sqrt{z-a}} + \chi \frac{b-a}{2\sqrt{z-b}\sqrt{z-a}}$$

for the inverse Joukowski transform

$$J_+^{-1}(z) = z - \sqrt{z-1}\sqrt{z+1}.$$

Sketch of Proof This theorem follows from Plemelj's lemma and the fact that

$$T_k(x) = \frac{J_{\downarrow}^{-1}(x)^k + J_{\downarrow}^{-1}(x)^{-k}}{2},$$

where

$$J_{\downarrow}^{-1}(x) = x - i\sqrt{1-x}\sqrt{1+x} = \lim_{\epsilon \downarrow 0} J_+^{-1}(x + i\epsilon).$$

□

To achieve the desired properties, we want ϕ to be bounded:

$$V_0 = 0 \quad \text{and} \quad \chi = 0.$$

We also want $\phi(z) \sim \frac{1}{z}$:

$$\frac{b-a}{8} V_1 = 1.$$

These two conditions give us a function

$$F(a, b) = \begin{pmatrix} V_0 \\ (b-a)V_1 - 8 \end{pmatrix}$$

for which we want to find a root. We can calculate V_0 and V_1 to high accuracy using the trapezium rule applied to

$$\int_{-1}^1 \frac{V'(M^{-1}(x))T_k(x)}{\sqrt{1-x^2}} dx = -2 \int_{-\pi}^{\pi} V'(M^{-1}(\cos \theta)) \cos k\theta d\theta.$$

This calculation is trivially differentiable with respect to a and b , hence we can easily apply Newton iteration to find a root of F . Convexity ensures that this root is unique [19].

Once (a, b) are computed, we calculate $\phi(z)$ by using the discrete cosine transform to calculate the Chebyshev coefficients of V' . We then have the equilibrium measure

$$d\mu = \frac{i}{2\pi} [\phi^+(x) - \phi^-(x)] dx = \frac{\sqrt{1 - M_{(a,b)}(x)^2}}{2\pi} \sum_{k=1}^{\infty} V_k U_{k-1}(M_{(a,b)}(x)) dx$$

where U_k are the Chebyshev polynomials of the second kind.

To calculate g , we compute an indefinite integral of ϕ [19]:

$$g(z) = \int^z \phi(z) dz = \frac{b-a}{4} \left[V_1 \left(\frac{J_+^{-1}(M_{(a,b)}(z))^2}{2} - \log J_+^{-1}(M_{(a,b)}(z)) \right) + \sum_{k=2}^{\infty} V_k \left(\frac{J_+^{-1}(M_{(a,b)}(z))^{k+1}}{k+1} - \frac{J_+^{-1}(M_{(a,b)}(z))^{k-1}}{k-1} \right) \right].$$

This formula was derived by mapping $J_+^{-1}(M_{(a,b)}(z))$ back to the unit circle, where it became a trivially integrable Laurent series. Note that g has a branch cut along $(-\infty, a)$ on which it satisfies:

$$g_+(x) - g_-(x) = 2\pi i.$$

Choosing (arbitrarily) $x \in (a, b)$, we calculate

$$\ell = V(x) - g_+(x) - g_-(x).$$

The numerically calculated g consists of approximating V_k using the discrete Cosine transform and truncating the sum. Due to analyticity, the errors in these computed coefficients are negligible, and the approximation of g is uniformly accurate in the complex plane. Hereafter, we treat the numerical g and the true g as equal.

3.2 Scaling constant for edge statistics

Associated with the equilibrium measure are the *Mhaskar–Rakhmanov–Saff numbers*. We re-express the constant as stated in [7] in terms of constants that we have already calculated: the support of the equilibrium measure and its Chebyshev coefficients. The equilibrium measure for the scaled potential $V(M_{(a,b)}^{-1}(x))$ has support $(-1, 1)$. Its equilibrium measure is

$$\begin{aligned} M_{(a,b)}^{-1}{}'(x) \psi(M_{(a,b)}^{-1}(x)) dx &= \frac{b-a}{2} \psi(M_{(a,b)}^{-1}(x)) dx = (b-a) \frac{\sqrt{1-x^2}}{4\pi} \sum_{k=1}^{\infty} V_k U_{k-1}(x) dx \\ &= \frac{\sqrt{1-x^2}}{2\pi} h(x) dx, \end{aligned}$$

as in [7, (3.3)]. We define the constant

$$\alpha = \left(\frac{h(1)^2}{2} \right)^{1/3} = \frac{1}{2} \left[(b-a) \sum_{k=1}^{\infty} k V_k \right]^{2/3}$$

as in [7, (3.10)]. The scaling constant is thus

$$c = \frac{2\alpha}{b-a} = (b-a)^{-1/3} \left[\sum_{k=1}^{\infty} k V_k \right]^{2/3}.$$

3.3 Lensing the RH problem

We can now rewrite Y to normalize the behaviour at infinity:

$$Y(z) = \begin{pmatrix} e^{\frac{n\ell}{2}} & \\ & e^{-\frac{n\ell}{2}} \end{pmatrix} T(z) \begin{pmatrix} e^{-ng} & \\ & e^{ng} \end{pmatrix} \begin{pmatrix} e^{-\frac{n\ell}{2}} & \\ & e^{\frac{n\ell}{2}} \end{pmatrix},$$

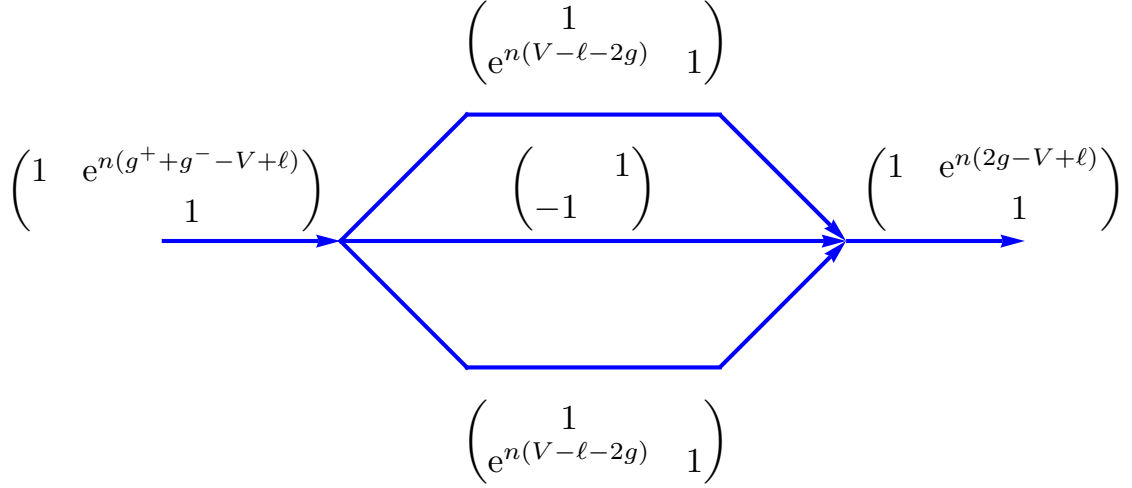


Figure 6: The jumps of T .

so that $T \sim I$ and has a branch cut along the unit interval, on which it satisfies

$$\begin{aligned}
T_+ &= T_- \begin{pmatrix} e^{n(g_- - g_+)} & e^{n(g_+ + g_- + \ell - V)} \\ & e^{n(g_+ - g_-)} \end{pmatrix} \\
&= T_- \begin{cases} \begin{pmatrix} 1 & e^{n(g_+ + g_- + \ell - V)} \\ & 1 \end{pmatrix} & x < a \text{ or } x > b \\ \begin{pmatrix} e^{n(g_- - g_+)} & & & 1 \\ & & & e^{n(g_+ - g_-)} \end{pmatrix} & a < x < b. \end{cases}
\end{aligned}$$

We appeal to properties of equilibrium measures (see [26]) to assert that

$$g_+(x) + g_-(x) + \ell - V < 0$$

for $x < a$ and $x > b$, thus those contributions of the jump matrix are isolated around a and b . On the other hand, $g_+ - g_-$ is imaginary between a and b , hence $e^{\pm n(g_+ - g_-)}$ becomes increasingly oscillatory on (a, b) . We wish to deform the RH problem into the complex plane to convert oscillations into exponential decay. To accomplish this, we introduce the lensing as in Figure 6, where we rewrite T by

$$T(z) = S(z) \begin{cases} \begin{pmatrix} 1 & \\ e^{n(V - \ell - 2g)} & 1 \end{pmatrix} & z \in \Sigma_+ \\ \begin{pmatrix} 1 & \\ e^{n(V - \ell - 2g)} & 1 \end{pmatrix} & z \in \Sigma_- \\ I & \text{otherwise.} \end{cases}$$

By substituting

$$g_+ = V - g_- - \ell,$$

we see that the oscillations have been removed completely from $\text{supp } \mu$:

$$\begin{aligned}
S_+ &= T_+ \begin{pmatrix} 1 & \\ -e^{n(V-\ell-2g_+)} & 1 \end{pmatrix} = T_+ \begin{pmatrix} 1 & \\ -e^{n(g_- - g_+)} & 1 \end{pmatrix} \\
&= T_- \begin{pmatrix} e^{n(g_- - g_+)} & 1 \\ & e^{n(g_+ - g_-)} \end{pmatrix} \begin{pmatrix} 1 & \\ -e^{n(g_- - g_+)} & 1 \end{pmatrix} \\
&= T_- \begin{pmatrix} 1 & \\ -1 & e^{n(g_+ - g_-)} \end{pmatrix} = S_- \begin{pmatrix} 1 & \\ -e^{n(V-\ell-2g_-)} & 1 \end{pmatrix} \begin{pmatrix} 1 & \\ -1 & e^{n(V-\ell-2g_-)} \end{pmatrix} \\
&= S_- \begin{pmatrix} 1 & \\ -1 & 1 \end{pmatrix}.
\end{aligned}$$

However, we have introduced new jumps on Γ_\uparrow and Γ_\downarrow , on which

$$S_+ = T_+ = T_- = S_- \begin{pmatrix} 1 & \\ e^{n(V-\ell-2g)} & 1 \end{pmatrix}.$$

3.4 Removing the connecting jump

We have successfully converted oscillations to exponential decay. However, to maintain accuracy of the numerical algorithm for large n , we must isolate the jumps to neighbourhoods of the endpoints a and b . Thus we require a function which satisfies the following RH problem:

$$N_+(x) = N_-(x) \begin{pmatrix} 1 & \\ -1 & 1 \end{pmatrix} \quad \text{for } a < x < b \quad \text{and} \quad N(\infty) = I.$$

The solution is [6]

$$N(z) = \frac{1}{2\nu(z)} \begin{pmatrix} 1 & i \\ -i & 1 \end{pmatrix} + \frac{\nu(z)}{2} \begin{pmatrix} 1 & -i \\ i & 1 \end{pmatrix} \quad \text{for } \nu(z) = \left(\frac{z-b}{z-a} \right)^{1/4};$$

i.e., $\nu(z)$ is a solution to

$$\nu_+(x) = i\nu_-(x) \quad \text{for } a < x < b \quad \text{and} \quad \nu(\infty) = 1.$$

An issue with using N as a parametrix is that it introduces singularities at a and b , hence we also introduce local parametrices to avoid these singularities. In the event that the equilibrium measure $\psi(x)$ has exactly *square root decay* at the edges, asymptotically accurate local parametrices are known. However, if the equilibrium measure has higher order decay (*à la* the higher-order Tracy–Widom distributions [4]), the asymptotically accurate local parametrices are only known in terms of a RH problem.

For numerical purposes, however, we do not need the parametrix to be asymptotically accurate: we achieve asymptotic accuracy by scaling the contours. Thus we introduce the *trivially constructed* local parametrices which satisfy the jumps of S in neighbourhoods of a and b :

$$P_a(z) = \left(\begin{array}{l} \begin{pmatrix} 1 & \\ 1 & 1 \end{pmatrix} \\ \begin{pmatrix} 1 & -1 \\ 1 & 1 \end{pmatrix} \\ \begin{pmatrix} 1 & -1 \\ 1 & 1 \end{pmatrix} \\ I \end{array} \begin{array}{l} \frac{\pi}{3} < \arg(z-a) < \pi \\ -\pi < \arg(z-a) < -\frac{\pi}{3} \\ -\frac{\pi}{3} < \arg(z-a) < 0 \\ \text{otherwise} \end{array} \right) \begin{pmatrix} e^{n(V-\ell-2g)} & \\ & e^{-n(V-\ell-2g)} \end{pmatrix}$$

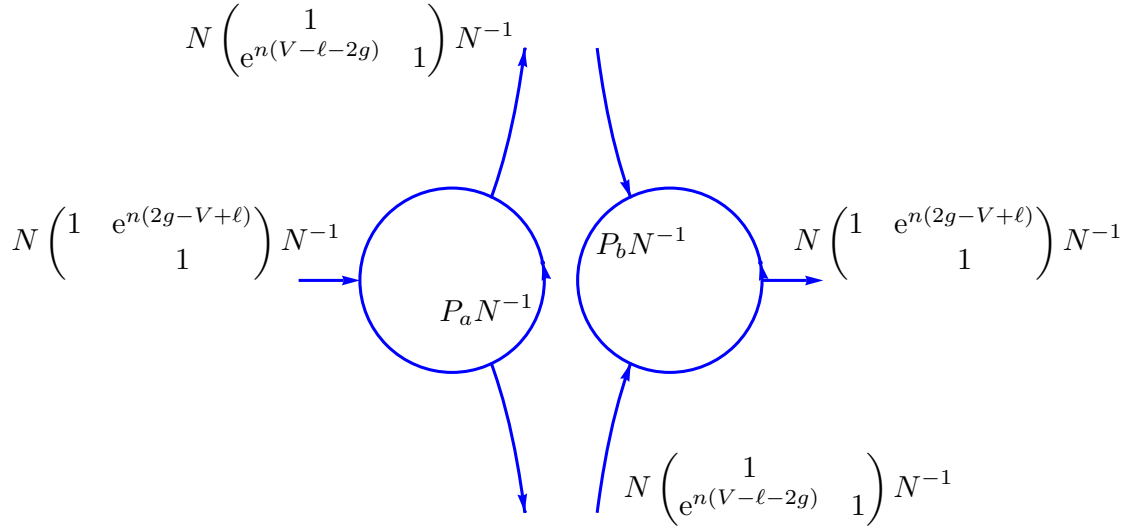


Figure 7: The jumps of Φ .

and

$$P_b(z) = \left(\left\{ \begin{array}{l} \begin{pmatrix} 1 & \\ -1 & 1 \end{pmatrix} & \frac{2\pi}{3} < \arg(z-b) < \pi \\ \begin{pmatrix} -1 & \\ 1 & 1 \end{pmatrix} & -\pi < \arg(z-b) < -\frac{2\pi}{3} \\ \begin{pmatrix} 1 & -1 \\ 1 & 1 \end{pmatrix} & -\frac{2\pi}{3} < \arg(z-b) < 0 \\ I & \text{otherwise} \end{array} \right. \right) \begin{pmatrix} e^{n(V-\ell-2g)} & \\ & e^{-n(V-\ell-2g)} \end{pmatrix}.$$

We can now write

$$S(z) = \Phi(z) \begin{cases} N(z) & |z-a| > r \text{ and } |z-b| > r \\ P_b(z) & |z-b| < r \\ P_a(z) & |z-a| < r \end{cases}$$

The final RH problem for Φ satisfies the jumps depicted in Figure 7.

In practice, we do not use infinite contours. We truncate contours when the jump matrix is, to machine precision, the identity matrix. In all cases we consider here, after proper deformations the jump matrices are C^∞ smooth and are exponentially decaying to the identity matrix for large z . The truncation of contours can be rigorously justified by solving a ‘nearby’ RH problem with truncated contours. For a full discussion of this see Section 5 and, in particular, Lemma 4 below. We can then deform the remaining contours to be line segments connecting their endpoints. The resulting jump contour consists only of affine transformations of the unit interval.

4 Numerical solution of Riemann–Hilbert problems

We have reduced the orthogonal polynomial RH problem to the form

$$\Phi^+(z) = \Phi^-(z)G(z), \quad z \in \Gamma, \quad \Phi(\infty) = I, \quad (1)$$

where $\Gamma = \Gamma^1 \cup \dots \cup \Gamma^L$ is a union of contours that are affine transformations of the unit interval: i.e., $M^i(\Gamma^i) = (-1, 1)$ for an affine transformation M^i . We use the notation $[G; \Gamma]$ to refer to this RH problem and $\Phi = [G; \Gamma]$ when Φ is the unique solution. Assume this solution has the form

$$\Phi(z) = I + \mathcal{C}_\Gamma U,$$

for some smooth function U . The RH problem (1) is converted into an equivalent singular integral equation (SIE) by substituting this assumed form into (1):

$$I + \mathcal{C}_\Gamma^+ U = (I + \mathcal{C}_\Gamma^- U)G. \quad (2)$$

We use the operator identity [6]

$$\mathcal{C}_\Gamma^+ - \mathcal{C}_\Gamma^- = I,$$

to rewrite (2)

$$U - \mathcal{C}_\Gamma^- U(G - I) = G - I. \quad (3)$$

It is well-known that the operators \mathcal{C}_Γ^\pm are bounded from $L^2(\Gamma)$ to itself for every contour we consider here. We use the notation

$$\mathcal{C}[G; \Gamma]U = U - \mathcal{C}_\Gamma^- U(G - I),$$

which is a well-defined bounded linear operator on $L^2(\Gamma)$ provided $G \in L^\infty(\Gamma)$.

Our numerical scheme consists of approximating U by a finite-dimensional sum of *mapped Chebyshev polynomials*. In other words, for $x \in \Gamma$ we approximate $U(x) \approx U\mathbf{m}(x)$, where we define

$$U\mathbf{m}(x) = U\mathbf{m}^i(x) = \sum_{k=0}^{m^i-1} U_k^i T_k(M^i(x)) \quad \text{for } x \in \Gamma^i,$$

for as-of-yet unknown coefficients $U_k^i \in \mathbb{C}^{2 \times 2}$. If we are given the coefficients, we can evaluate $\mathcal{C}[G; \Gamma]U\mathbf{m}$ *pointwise* by using an exact expression for the Cauchy transform of our basis:

Proposition 1 [20]

$$\mathcal{C}_{\Gamma^i}[T_k \circ M^i](z) = \mathcal{C}_{(-1,1)} T_k(M^i(z))$$

Sketch of Proof Follows from Plemelj's lemma:

$$\mathcal{C}_{(-1,1)} T_k(M^i(\infty)) = \mathcal{C}_{(-1,1)} T_k(\infty) = 0$$

and

$$\left[\mathcal{C}_{(-1,1)}^+ - \mathcal{C}_{(-1,1)}^- \right] T_k(M^i(x)) = T_k(M^i(x)).$$

□

Theorem 2 [20, 21] *Define*

$$\psi_k(z) = \frac{2}{i\pi} \begin{cases} \operatorname{arctanh} z & \text{for } k = 0 \\ \frac{z^{1+2\lfloor -k/2 \rfloor + k}}{(1-z^2)(1+2\lfloor -k/2 \rfloor)} {}_2F_1\left(\frac{1, 1}{\frac{3}{2} + \lfloor -k/2 \rfloor}; \frac{z^2}{z^2-1}\right) & \text{for } k < 0 \\ z^k (\operatorname{arctanh} z - \operatorname{arctanh} z^{-1}) \\ + \frac{z^{k-1-2\lfloor (k+1)/2 \rfloor}}{(1-z^{-2})(1+2\lfloor (k+1)/2 \rfloor)} {}_2F_1\left(\frac{1, 1}{\frac{3}{2} + \lfloor (k+1)/2 \rfloor}; \frac{z^{-2}}{z^{-2}-1}\right) & \text{for } k > 0, \end{cases}$$

where ${}_2F_1$ is the hypergeometric function [18]. Then

$$\mathcal{C}T_k(z) = -\frac{1}{2} [\psi_k(J_+^{-1}(z)) + \psi_{-k}(J_+^{-1}(z))],$$

where

$$J_+^{-1}(z) = z - \sqrt{z-1}\sqrt{z+1}$$

is again an inverse of the Joukowski transform $J(z) = \frac{1}{2}(z + z^{-1})$.

Sketch of Proof This also follows from Plemelj's lemma after mapping to the unit circle:

$$T_k(J(z)) = \frac{z^k + z^{-k}}{2},$$

and relating the Taylor series of $\operatorname{arctanh} z$ to the hypergeometric function. □

We now choose the coefficients U_k^i by enforcing (3) to hold pointwise at a collection of $N = |\mathbf{m}| = m^1 + \dots + m^\ell$ points. In other words, we choose points $\{z_1^i, \dots, z_{m_i}^i\}$ lying on each Γ_i , and solve the $4N \times 4N$ linear system

$$\mathcal{C}[G; \Gamma] U_{\mathbf{m}}(z_k^i) = G(z_k^i) - I. \quad (4)$$

We choose *mapped Chebyshev points* for the points:

$$\{z_1^i, \dots, z_{m_i}^i\} = \left\{ M^{i-1}(-1), M^{i-1} \left(\cos \pi \left[1 - \frac{1}{m_i - 1} \right] \right), \dots, M^{i-1}(1) \right\}.$$

This means every junction point of Γ is included in the collocation system, with multiplicity the number of contours emanating from the junction point. We denote these repeated points by

$$\{\xi + 0e^{i\theta_1}, \dots, \xi + 0e^{i\theta_L}\}$$

where $\theta_1, \dots, \theta_L$ are the angles in which the components of Γ that include ξ as a junction point emanate from ξ . But, as seen in Theorem 2, the Cauchy transform for our basis blows up at such points! To overcome this discrepancy, we assume that the solution satisfies the *zero sum condition*:

Definition 2 $U_{\mathbf{m}}$ satisfies the zero sum condition if, at every junction point ζ , it satisfies

$$\sum p_i U_{\mathbf{m}}^i(\zeta) = 0$$

where $p_i = -1$ if the left endpoint of Γ^i is ζ , $p_i = 1$ if the right endpoint of Γ^i is ζ and $p_i = 0$ if ζ is not an endpoint of Γ^i .

We can define an alternate expression for the Cauchy transform at the junction points:

Definition 3 For z not an endpoint of Γ^i ,

$$\tilde{\mathcal{C}}_{\Gamma^i}[T_k \circ M^i](z) = \mathcal{C}_{\Gamma^i}[T_k \circ M^i](z).$$

Otherwise, for z_L^i the left endpoint of Γ^i and z_R^i the right endpoint, if $\theta \neq \theta_i$ define

$$\begin{aligned} \tilde{\mathcal{C}}_{\Gamma^i}[T_k \circ M^i](z_L^i + 0e^{i\theta}) &= a_k^L + ir_k^L \arg(-e^{i(\theta - \theta_i)}) \\ \tilde{\mathcal{C}}_{\Gamma^i}[T_k \circ M^i](z_R^i + 0e^{i\theta}) &= a_k^R + ir_k^R \arg(e^{i(\theta - \theta_i)}) \end{aligned}$$

for

$$\begin{aligned} a_k^L &= (-1)^k \frac{\log 2}{2\pi i} + \frac{(-1)^k}{i\pi} [\mu_{k-1}(-1) + \mu_k(-1)] + r_k^L \log |M^{i'}|, r_k^L = -\frac{(-1)^k}{2\pi i}, \\ a_k^R &= -\frac{\log 2}{2\pi i} + \frac{1}{i\pi} [\mu_{k-1}(1) + \mu_k(1)] + r_k^R \log |M^{i'}|, r_k^R = \frac{1}{2\pi i}, \end{aligned}$$

where

$$\mu_k(z) = \sum_{j=1}^{\lfloor \frac{k+1}{2} \rfloor} \frac{z^{2j-1}}{2j-1}.$$

When $\theta = \theta_i$ define

$$\tilde{\mathcal{C}}_{\Gamma^i}^{\pm}[T_k \circ M^i](z_L^i + 0e^{i\theta_i})$$

by the appropriate limits.

The usefulness of this alternative definition is that it is equivalent to the standard Cauchy transform for functions which satisfy the zero sum condition:

Lemma 1 [22] *If $U_{\mathbf{m}}$ satisfies the zero sum condition, then*

$$\tilde{\mathcal{C}}U_{\mathbf{m}}(z) = \mathcal{C}U_{\mathbf{m}}(z).$$

Sketch of Proof Let ζ be a junction point of Γ . From the asymptotic behaviour of $\operatorname{arctanh} z$, we see near ζ that if ζ is an endpoint of Γ^i ,

$$\mathcal{C}_{\Gamma^i}[T_k \circ M^i](z) \sim -\frac{p_i}{2\pi i} \log |z - z_L^i| + C_{\theta,k}^i$$

where $\theta = \arg(z - \zeta)$ and p_i is defined as in Definition 2. If ζ is not a junction point of Γ^i , then

$$\mathcal{C}_{\Gamma^i}[T_k \circ M^i](z) \sim \mathcal{C}_{\Gamma^i}[T_k \circ M^i](\zeta) =: C_{\theta,k}^i,$$

(where $C_{\theta,k}^i$ is θ independent). Thus,

$$\begin{aligned} \mathcal{C}U_{\mathbf{n}}(z) &= \sum_i \sum_k U_k^i \mathcal{C}_{\Gamma^i}[T_k \circ M^i](z) \sim -\sum_i p_i U^i(\zeta) \frac{1}{2\pi i} \log |z - z_L^i| + \sum_i \sum_k C_{\theta,k}^i \\ &= \sum_i \sum_k C_{\theta,k}^i; \end{aligned}$$

since the zero sum condition ensures that

$$\sum_i p_i U^i(\zeta) = 0.$$

The remaining constant $C_{\theta,k}^i$, which we refer to as the *finite part*, are precisely the constants we defined above. \square

Thus, assuming the coefficients U_k^i are in the space so that $U_{\mathbf{m}}$ satisfies the zero sum condition, we can replace (4) by

$$\tilde{\mathcal{C}}[G, \Gamma]U_{\mathbf{m}}(z_k^i) = G(z_k^i) - I. \quad (5)$$

This is justified by the following:

Lemma 2 [22] *If the linear system (5) is nonsingular, then the calculated $U_{\mathbf{m}}$ satisfy the zero sum condition.*

Sketch of Proof Let ζ be a junction point, and assume for simplicity that $p_i = 1$ or 0 and Γ_i are ordered by increasing arguments θ_i . Define

$$\Phi_i^\pm = I + \tilde{C}^\pm U_{\mathbf{m}}(\zeta + 0e^{i\theta_i}),$$

and define

$$G_i = G(\zeta + 0e^{i\theta_i})$$

(i.e., the limit of the jump along Γ^i). The collocation system imposes

$$\Phi_i^+ = \Phi_i^- G_i.$$

But the definition of \tilde{C} imposes that

$$\Phi_{i+1}^- = \Phi_i^+ + (\theta_{i+1} - \theta_i)S \quad \text{and} \quad \Phi_1^- = \Phi_L^+ + (\theta_1 + 2\pi - \theta_L)S$$

for

$$S = - \sum_i p_i \frac{U_i(0)}{2\pi i}.$$

These equations give

$$\begin{aligned} \Phi_L^+ &= \Phi_L^+ G_1 \cdots G_L + S \left[(\theta_1 + 2\pi - \theta_L) G_1 \cdots G_L + \sum_{i=2}^L (\theta_i - \theta_{i-1}) G_i \cdots G_L \right] \\ &= \Phi_L^+ + S \left[(\theta_1 + 2\pi - \theta_L) I + \sum_{i=2}^L (\theta_i - \theta_{i-1}) G_i \cdots G_L \right] \end{aligned}$$

where we use the well-posedness of the RH problem:

$$G_1 \cdots G_L = I.$$

If

$$(\theta_1 + 2\pi - \theta_L) I + \sum_{i=2}^L (\theta_i - \theta_{i-1}) G_i \cdots G_L$$

is nonsingular (the *nonsingular junction condition*), then $S = 0$, implying the zero sum condition.

Now suppose the nonsingular junction condition is not satisfied, and we replace the condition in the collocation system that

$$\Phi_L^+ = \Phi_L^- G_L,$$

with $S = 0$. We then have

$$\Phi_{i+1}^- = \Phi_i^+ \quad \text{and} \quad \Phi_1^- = \Phi_L^+.$$

Thus

$$\begin{aligned} \Phi_L^- G_L &= \Phi_{L-1}^+ G_{L-1} G_L = \cdots = \Phi_{L-1}^+ G_1 \cdots G_{L-1} G_L \\ &= \Phi_L^+, \end{aligned}$$

and the removed condition is still satisfied. In other words, the two linear systems are *equivalent*. □

In conclusion, the fact that the linear system is nonsingular implies that the numerically constructed

$$\Phi_{\mathbf{m}}(z) = I + \mathcal{C}U_{\mathbf{m}}(z)$$

is analytic off Γ and satisfies the correct jumps at the collocation points. We can thus recover approximations to orthogonal polynomials from $\Phi_{\mathbf{m}}$ by undoing the transformations $Y \mapsto T \mapsto S \mapsto \Phi$.

We have one last task: we need to scale the contours so that the numerical algorithm remains accurate for all choices of n .

4.1 Spaces

We follow [23] and interpret the operator defined by applying $\tilde{\mathcal{C}}_{\Gamma}$ and sampling the resulting function at $\{z_k^i\}$ as mapping of piecewise polynomials to piecewise polynomials. The sampled function at the values $\{z_k^i\}$ can be identified with its unique piecewise-polynomial interpolant and we use $\mathcal{I}_{\mathbf{m}}$ to denote this interpolation operator. Define $L_{m_i}^2(\Gamma^i)$ to be the space of matrices with entries being m_i th order polynomials. When $\Gamma = \Gamma^1 \cup \dots \cup \Gamma^L$ has intersection points we define

$$L_{\mathbf{m}}^2(\Gamma) = \bigoplus_{i=1}^L L_{m_i}^2(\Gamma^i).$$

We define $L_{\mathbf{m},z}^2(\Gamma)$ to be the closed subspace of $L_{\mathbf{m}}^2(\Gamma)$ consisting of functions that satisfy the zero sum condition. Thus $\mathcal{I}_{\mathbf{m}}\tilde{\mathcal{C}}_{\Gamma}$ is a well-defined linear operator from $L_{\mathbf{m},z}^2(\Gamma)$ to $L_{\mathbf{m}}^2(\Gamma)$. As is mentioned in [23], $\mathcal{I}_{\mathbf{m}}\tilde{\mathcal{C}}[G; \Gamma]$ maps to a proper subspace of $L_{\mathbf{m}}^2(\Gamma)$.

For each component contour Γ^i and $k \in \mathbb{N}^+$ we define $H^k(\Gamma^i)$ and $W^{k,\infty}(\Gamma^i)$ in the usual way [23]. For the contour Γ

$$H^k(\Gamma) = \bigoplus_{i=1}^L H^k(\Gamma^i), \quad W^{k,\infty}(\Gamma) = \bigoplus_{i=1}^L W^{k,\infty}(\Gamma^i).$$

Define $H_z^k(\Gamma)$ to be the close subspace $H^k(\Gamma)$ consisting of functions whose $(k-1)$ th-order derivatives each satisfy the zero sum condition. Finally, for a Banach spaces X we use $\mathcal{L}(X)$ to denote the Banach space of operators on X with the induced operator norm.

5 Uniform approximation

In this section we describe how the convergence of the numerical approximation of RH problems can be made uniform in a parameter. We also refer to this uniformity as *asymptotic stability* of the numerical method. In the case of orthogonal polynomials, the relevant parameter is n , the degree of the polynomial. We refer to the results of [23]. We assume that we have a sequence of RH problems $[G_n; \Gamma_n]$ depending on the parameter n . The theory of [23] requires some assumptions on Γ_n . Assume

$$\Gamma_n = \Omega_n^1 \cup \dots \cup \Omega_n^l,$$

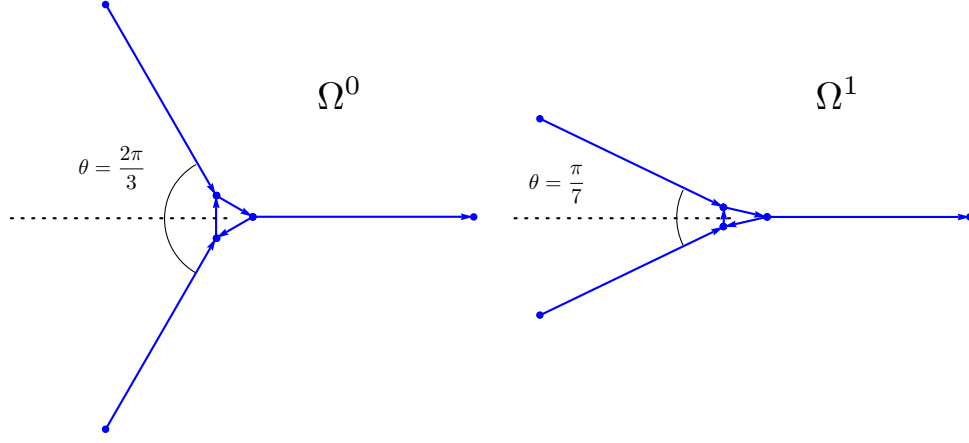


Figure 8: The pre-scaled Ω^0 used for non-degenerate endpoints and the pre-scaled Ω^1 used for first order degenerate endpoints.

where $\{\Omega_n^j\}_{j=1}^l$ are mutually disjoint and have the form

$$\Omega_n^j = \alpha_n^j \Omega^j + \beta_n^j.$$

We assume Γ_n is the disjoint union of contours, each of which is an affine transformation of a fixed contour. Once we have this separation of Γ_n we attempt to solve the RH problem $[G_n; \Gamma_n]$ in an iterative way. We define the restricted jumps $G_n^j = G_n|_{\Omega_n^j}$ and the jumps after variable change $H_n^j(k) = G_n^j(\alpha_n^j k + \beta_n^j)$, $k \in \Omega_j$. The following result can be found in [23]. For notational simplicity we suppress the dependence on n . But it is important to note in the general case every function, but no domain, will depend on n .

Lemma 3 (Scaled and shifted solver) *Assume $\tilde{\Phi}_1 = [H^1; \Omega_1]$ and define $\Phi_1 = \tilde{\Phi}_1 \left(\frac{z - \beta^1}{\alpha^1} \right)$. Furthermore, for each $j = 2, \dots, l$ define $\Phi_{i,j}(k) = \Phi_i(\alpha^j k + \beta^j)$ and set*

$$\tilde{\Phi}_j = [\Phi_{j-1,j} \cdots \Phi_{1,j} H_j \Phi_{1,j}^{-1} \cdots \Phi_{j-1,j}^{-1}; \Omega_j], \quad \Phi_j(z) = \tilde{\Phi}_j \left(\frac{z - \beta^j}{\alpha^j} \right).$$

Then $\Phi = \Phi_1 \cdots \Phi_l$ solves $[G_n; \Gamma_n]$.

This lemma states that we can treat each disjoint contour separately. We first solve a RH problem on one contour and modify the remaining jumps with the solution. This process is repeated until all contours are taken account of.

We use the following rule of thumb to determine the proper scalings α_n^j :

Assumption 1 *If the jump matrix G has a factor $e^{n\theta}$ and β^j corresponds to a q th order stationary point (i.e., $\theta(z) \sim C(z - \beta^j)^q$), then the scaling which achieves asymptotic stability is (a constant multiple of) $\alpha_n^j = n^{-1/q}$.*

In the case of a non-degenerate equilibrium measure, $g(z) \sim c_a(z - a)^{3/2}$ and $g(z) \sim c_b(z - b)^{3/2}$; we thus scale like $n^{-2/3}$:

$$\Omega_n^1 = -n^{-2/3} \Omega^0 + a \quad \text{and} \quad \Omega_n^2 = n^{-2/3} \Omega^0 + b,$$

where Ω^0 is depicted in Figure 8, and the angle of the contours are chosen to match the direction of steepest descent. In the first order degenerate case (eg., $V(x) = \frac{x^2}{5} - \frac{4}{15}x^3 + \frac{x^4}{20} + \frac{8}{5}x$), $g(z) \sim c_b(z - b)^{7/2}$ and so we scale like $n^{-7/2}$ at the degenerate endpoint:

$$\Omega_n^1 = n^{-2/3}\Omega^0 + a \quad \text{and} \quad \Omega_n^2 = n^{-7/2}\Omega^1 + b,$$

where Ω^1 is depicted in Figure 8 (the angle is sharper to attach to the new direction of steepest descent). Higher order degenerate equilibrium measures will require higher order scalings, but this can be determined systematically by investigating the number of vanishing derivatives of the equilibrium measure.

This is the final form of the RH problem that we used in the numerical calculations of Section 2. The remainder of the paper is concerned with proving that this scaled and shifted RH problem achieves *asymptotic accuracy*, i.e., the error does not grow as n becomes large.

5.1 Conditions for uniform approximation

A significant question is whether each of these smaller RH problems is solvable. From a practical numerical standpoint this possible issue does not seem to affect the conditioning of the method. From a theoretical standpoint this question is settled for large n in [23] provided $\alpha_n^j \rightarrow 0$ for all j as $n \rightarrow \infty$ with some mild restrictions on β_n^j .

Assumption 2 *Assume that the jump matrix G is C^∞ when restricted to each component Γ^i of Γ and decays to the identity matrix faster than any polynomial at each isolated endpoint of Γ and at ∞ if $\infty \in \Gamma$.*

This is true in all cases we consider here. The following lemma is proved in [23].

Lemma 4 (Contour truncation) *For every $\epsilon > 0$ there exists an matrix-valued function G_ϵ and a bounded contour Γ_ϵ such that*

- $G_\epsilon = I$ on $\Gamma \setminus \Gamma_\epsilon$,
- $\|G_\epsilon - G\|_{L^2(\Gamma) \cap L^\infty(\Gamma)} < \epsilon$, and
- $\|\mathcal{C}[G; \Gamma] - \mathcal{C}[G_\epsilon; \Gamma_\epsilon]\|_{\mathcal{L}(L^2(\Gamma))} < \epsilon \|\mathcal{C}_\Gamma^-\|_{\mathcal{L}(L^2(\Gamma))}$.

Note that when the jump matrix G is the identity matrix then the solution of the RH problem is analytic across the jump. In practice we truncate infinite contours to finite contours when the jump matrix is within machine precision of the identity matrix. The lemma justifies this process and we always assume Γ is bounded.

The following theorem is the fundamental result of [23] and gives the required tools to address the accuracy of the Riemann–Hilbert numerical methods for orthogonal polynomials for arbitrarily large n :

Theorem 3 *Assume*

- $\mathcal{C}[H_n^j, \Omega^j]^{-1}$ exists and the norm $\|\mathcal{C}[H_n^j, \Omega^j]^{-1}\|_{\mathcal{L}(L^2(\Omega^j))} \leq C$ for all j and n ,
- $\|H_n^j\|_{W^{k,\infty}(\Omega^j)} \leq C$ for all j and n , and
- $\alpha_n^j \rightarrow 0$ as $n \rightarrow \infty$.

Then for n sufficiently large

- The algorithm of Lemma 3 has solutions at each stage,
- The approximation U_{n,m_j}^j of U_n^j , the solution of the SIE at stage j in the algorithm of Lemma 3 converges in L^2 norm, uniformly in n provided $m_i \rightarrow \infty$ for all $i \leq j$.

The theorem states that if the contours Γ_n^j all have decaying measure then local boundedness properties on each of the contours can be made global for n large. As we will see below, bounding the $W^{k,\infty}$ norms of the matrices H_n^j is often straightforward and the boundedness properties of the inverse operator follows from the asymptotic analysis of the RH problem.

Remark If $\Gamma_n = \Omega_n^1$ consists of just one scaled contour then the restriction that $\alpha_n^1 \rightarrow 0$ can be removed due to the fact that $z = \alpha_n^1 k + \beta_n^1$ is a conformal change of variables for the whole problem and this leaves the Cauchy integral operators invariant.

Remark Similar results hold when the bounds in Theorem 3 are known for a ‘nearby’ RH problem. In this case bounds on the nearby RH problem give slightly weaker convergence properties that can still be seen to be uniform in an appropriate sense [23].

5.2 The classical Airy parametrix

In this section we present the deformation and asymptotic solution of the RH problem that is performed in the asymptotic analysis of the RH problem for orthogonal polynomials. The results from this section can be found in [6]. For brevity of presentation in this section we deal with potentials of the form $V(x) = x^{2m}$. For the asymptotic analysis and deformations in the more case of $V(x)$ polynomial see [10, 11, 8, 9].

A sectionally analytic, matrix-valued function $\hat{\Phi}$ is constructed explicitly out of the Airy function $\text{Ai}(s)$ and its derivative such that $T\hat{\Phi}^{-1} \rightarrow I$ as $n \rightarrow \infty$ where T is the solution of the original but deformed RH problem. The RH problem for the error $E = T\hat{\Phi}^{-1}$ has smooth solutions and is a near identity RH problem in the sense that the associated singular integral operator is expressed in the form $I - K_n$ with $\|K_n\|_{L^2} \rightarrow 0$ as $n \rightarrow \infty$. Thus E can be computed via a Neumann series for sufficiently large n .

The deformation proceeds much in the same way as Section 3.4, except we replace P_a and P_b with new functions ψ_a and ψ_b that are constructed out of the Airy function. We now construct these functions. As an intermediate step, define

$$\Psi(s) = \begin{cases} \begin{pmatrix} \text{Ai}(s) & \text{Ai}(\omega^2 s) \\ \text{Ai}'(s) & \omega^2 \text{Ai}'(\omega^2 s) \end{pmatrix} e^{-i\frac{\pi}{6}\sigma_3} & 0 < \arg s < \frac{2\pi}{3} \\ \begin{pmatrix} \text{Ai}(s) & \text{Ai}(\omega^2 s) \\ \text{Ai}'(s) & \omega^2 \text{Ai}'(\omega^2 s) \end{pmatrix} e^{-i\frac{\pi}{6}} & \frac{2\pi}{3} < \arg s < \pi \\ \begin{pmatrix} \text{Ai}(s) & \text{Ai}(\omega^2 s) \\ \text{Ai}'(s) & \omega^2 \text{Ai}'(\omega^2 s) \end{pmatrix} e^{-i\frac{\pi}{6}\sigma_3} \begin{pmatrix} 1 & \\ -1 & 1 \end{pmatrix} & \pi < \arg s < \frac{4\pi}{3} \\ \begin{pmatrix} \text{Ai}(s) & -\omega^2 \text{Ai}(\omega s) \\ \text{Ai}'(s) & -\text{Ai}'(\omega s) \end{pmatrix} e^{-i\frac{\pi}{6}\sigma_3} \begin{pmatrix} 1 & \\ 1 & 1 \end{pmatrix} & \frac{4\pi}{3} < \arg s < 2\pi \end{cases}$$

$$\omega = e^{\frac{2\pi i}{3}}.$$

The relations

$$\begin{aligned} \text{Ai}(s) + \omega \text{Ai}(\omega s) + \omega^2 \text{Ai}(\omega^2 s) &= 0, \\ \text{Ai}'(s) + \omega^2 \text{Ai}'(\omega s) + \omega \text{Ai}'(\omega^2 s) &= 0, \end{aligned}$$

can be used to show that $\Psi(s)$ satisfies the following jump conditions

$$\Psi^+(s) = \Psi^-(s) \begin{cases} \begin{pmatrix} 1 & 1 \\ & 1 \end{pmatrix} & s \in \gamma_1 \\ \begin{pmatrix} 1 & \\ 1 & 1 \end{pmatrix} & s \in \gamma_2 \\ \begin{pmatrix} & 1 \\ -1 & \end{pmatrix} & s \in \gamma_3 \\ \begin{pmatrix} 1 & \\ 1 & 1 \end{pmatrix} & s \in \gamma_4 \end{cases}.$$

See Figure 9 for γ_i , $i = 1, \dots, 4$.

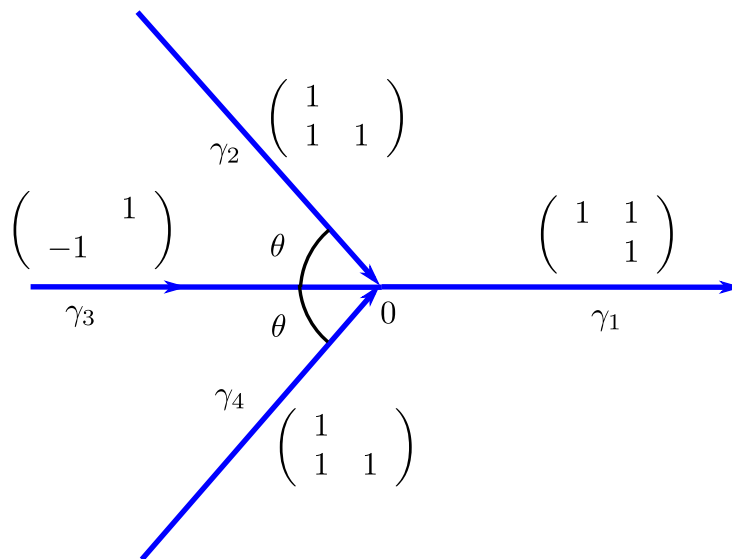


Figure 9: The jump contours for Ψ with jump matrices. We include $\theta > 0$ in the figure for concreteness but its exact value is not needed below.

Since we only consider V even in this section, the equilibrium measure is supported on a symmetric interval $[-a, a]$ for $a > 0$. Define

$$\begin{aligned} \Lambda(z) &= \frac{3}{2}\varphi(z)(z-a)^{-3/2}, \quad \lambda(z) = (z-a)(\Lambda(z))^{2/3}, \\ \varphi(z) &= \frac{1}{2}(V(z) - \ell) - g(z). \end{aligned}$$

It follows from the branching properties of φ that Λ and λ are analytic in a neighbourhood of a . Furthermore, since $\lambda(a) = 0$ and $\lambda'(a) = (\Lambda(a))^{2/3} \neq 0$ we use it as a conformal change of variables mapping a neighbourhood of $z = a$ into a neighbourhood of the origin. More precisely, fix an $\epsilon > 0$ and define $O_a = \lambda^{-1}(\{|z| < \epsilon\})$.

Define

$$\begin{aligned} \psi_a(z) &= L(z)\Psi(n^{2/3}\lambda(z))e^{n\varphi(z)\sigma_3}, \\ L(z) &= \begin{pmatrix} 1 & -1 \\ -i & -i \end{pmatrix} \sqrt{\pi}e^{i\frac{\pi}{6}}n^{\sigma_3/6}((z+a)\Lambda^{2/3}(z))^{\sigma_3/4}. \end{aligned}$$

ψ_a solves the local RH problem shown in Figure 10(b). The symmetry of $V(x)$ implies that $\psi_{-a}(z) = \sigma_3\psi_a(-z)\sigma_3$ satisfies the jumps shown in Figure 10(a). We are ready to define the

full parametrix

$$\hat{\Phi}(z) = \begin{cases} \psi_a(z) & z \in O_a \\ \psi_{-a}(z) & z \in -O_a \\ N(z) & \text{otherwise} \end{cases}.$$

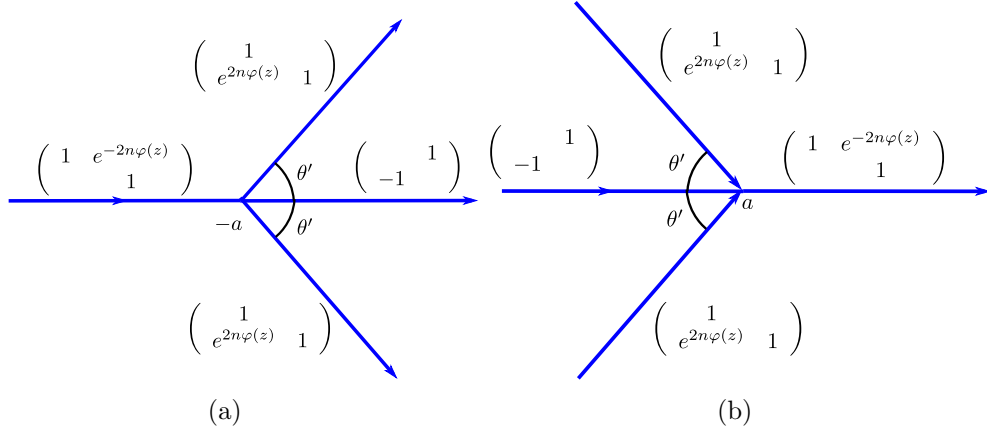


Figure 10: The local parametrices near $z = a, -a$. As above $\theta' > 0$ is included for concreteness but its exact value is not needed. (a) The jump contours for ψ_{-a} with jump matrices. (b) The jump contours for ψ_a with jump matrices.

We will need a result concerning the asymptotics of the Airy function

$$\begin{aligned} \text{Ai}(s) &= \frac{1}{2\sqrt{\pi}} s^{-1/4} e^{-\frac{2}{3}s^{3/2}} \left(1 + \mathcal{O}\left(\frac{1}{s^{3/2}}\right) \right), \\ \text{Ai}'(s) &= -\frac{1}{2\sqrt{\pi}} s^{3/4} e^{-\frac{2}{3}s^{3/2}} \left(1 + \mathcal{O}\left(\frac{1}{s^{3/2}}\right) \right), \end{aligned}$$

as $s \rightarrow \infty$ and $|\arg s| < \pi$. These asymptotics, along with the definition of $\lambda(z)$, can be used to show

$$\psi_a(z)N^{-1}(z) = I + \mathcal{O}(n^{-1}), \quad z \in \partial O_a, \quad (6)$$

$$\psi_{-a}(z)N^{-1}(z) = I + \mathcal{O}(n^{-1}), \quad z \in \partial O_{-a}, \quad (7)$$

as $n \rightarrow \infty$ uniformly in z provided $O_a \cup O_{-a}$ is contained in a sufficiently narrow strip containing the real line. See [6] for the details.

We take the RH problem for T in Figure 6 and label ∂O_a and ∂O_{-a} . Note that without loss of generality we take O_a and O_{-a} to be open balls around a and $-a$, respectively. Analyticity allows us to deform any open, simply connected set containing a or $-a$ to a ball.

Since ψ_a and ψ_{-a} solve the RH problem locally in O_a and O_{-a} , respectively, the function $E = T\hat{\Psi}^{-1}$ is analytic in O_a and O_{-a} . See Figure 11 for the jump contour, Ω , and jump matrix, J , for the RH problem for E . It is shown in [6] using (6) that the jump matrix for this RH problem tends uniformly to the identity matrix as $n \rightarrow \infty$, again provided that all contours are in sufficiently small neighbourhood of the real line. Thus

$$\|I - \mathcal{C}[J; \Omega]\|_{\mathcal{L}(L^2(\Omega))} = \mathcal{O}(n^{-1}),$$

and a Neumann series will produce the unique solution u of $\mathcal{C}[J; \Omega]u = J - I$. T is found via the expression

$$T(z) = (I + \mathcal{C}_\Omega u(z))\hat{\Psi}(z).$$

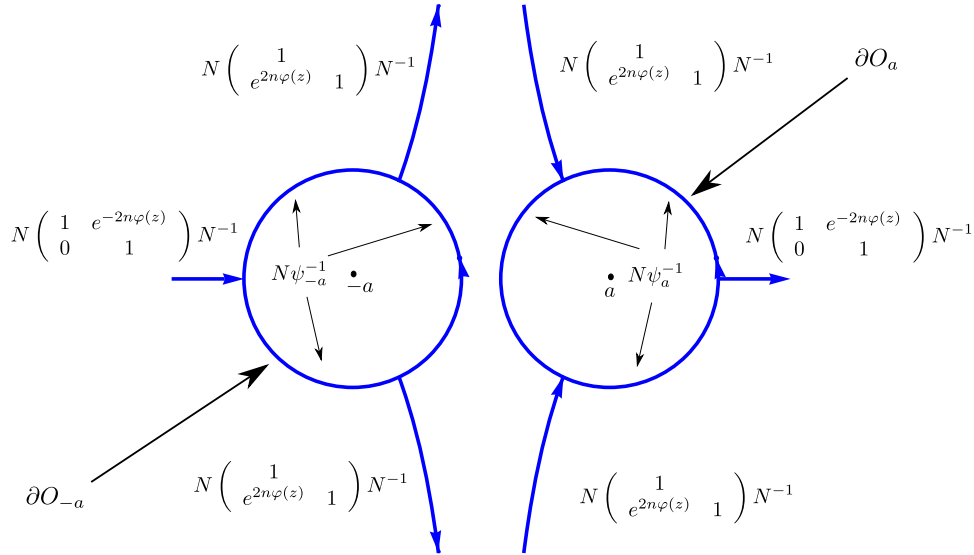


Figure 11: The jump contours Ω for the error E . The jump matrix J for E which is taken as the piecewise definition as shown.

5.3 Obtaining the bounds in Theorem 3

To apply Theorem 3 one has to first identify the correct scalings for the contours and second, establish bounds on the relevant operator norms and function derivatives.

5.3.1 The RH problem for E

In this case, we consider numerically solving the RH problem for E , rather than scaling and shifting the contours as we do in practice. This simplifies the proof of uniform approximation considerably, at the expense of no longer allowing for degenerate potentials, and requiring significantly more knowledge in the construction of the RH problem.

Take $\Gamma_n = \Omega$; that is, we do not scale the contour. The near-identity nature of the RH problem allows us to avoid any scaling of the problem. Using the asymptotic expansions for the derivatives of Airy functions one can show that

$$\|J - I\|_{W^{k,\infty}(\Omega) \cap H^k(\Omega)} = \mathcal{O}(n^{-1}).$$

Furthermore, the fact that $\|\mathcal{C}[J; \Omega]^{-1}\|_{\mathcal{L}(L^2(\Omega))} < C$ follows easily from the Neumann series argument already given. Thus we expect the numerical method to uniformly approximate solutions of this RH problem for small and arbitrarily large n .

To demonstrate the convergence properties of the solution for large n we use the following procedure. Let $U_{\mathbf{m}}$ denote the approximation of u obtained using the numerical method for RH problems discussed above with $m = |\mathbf{m}|$ collocation points per contour. When we break up Ω into both its non-self-intersecting components and components that can be represented by affine transformations of the unit interval we end up with 14 contours. Thus, we use a total of $14m$ collocation points. We solve the RH problem with $m = 10$ and then again with $m = 20$. We sample U_{10} at each collocation point for U_{20} and measure the maximum difference at these collocations points. We define this difference to be the *Cauchy error*. Figure 12 demonstrates that the error decreases as $n \rightarrow \infty$.

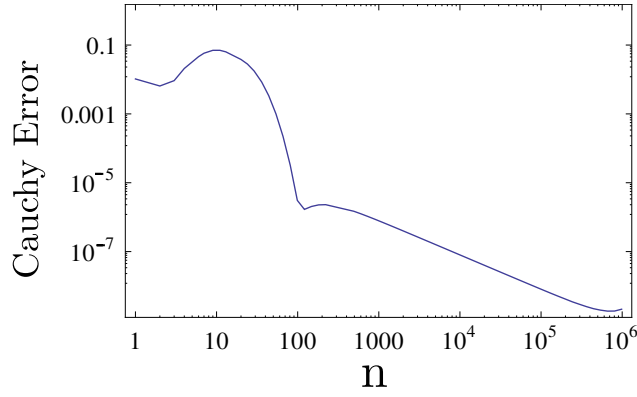


Figure 12: The *Cauchy error* between U_{10} and U_{20} as $n \rightarrow \infty$. This plot indicates that it takes fewer collocation points to approximate E as n increases.

5.3.2 The RH problem for Φ

The RH problem that we use in practice, Φ , is of a fundamentally simpler form. No additional special functions (e.g Airy functions) are needed and yet the contours are located away from the stationary points, a and b (we return here to allowing general potentials). All deformations are performed by a reordering and analytic continuation of previously defined functions.

Assume we are in the non-degenerate case. Represent

$$\Gamma_n = \Omega_n^1 \cup \Omega_n^2,$$

for

$$\Omega_n^1 = n^{-2/3}\Omega^0 + a \quad \text{and} \quad \Omega_n^2 = n^{-2/3}\Omega^0 + b.$$

Unfortunately, we have an issue with the jumps on these scaled contours: as $n \rightarrow \infty$, they approach the unbounded singularities of $N(z)$, violating the conditions of Theorem 3. However, we can expand

$$\begin{aligned} N(a - zn^{-2/3}) &= \frac{n^{1/6}}{2} \left(\frac{b-a}{z} \right)^{\frac{1}{4}} \begin{pmatrix} 1 & -i \\ i & 1 \end{pmatrix} + \frac{n^{-1/6}}{2(b-a)} \left(\frac{b-a}{z} \right)^{\frac{3}{4}} \begin{pmatrix} 1 & i \\ -i & 1 \end{pmatrix} + \mathcal{O}(n^{-\frac{1}{2}}), \\ N(a - zn^{-2/3})^{-1} &= \frac{n^{1/6}}{2} \left(\frac{b-a}{z} \right)^{\frac{1}{4}} \begin{pmatrix} 1 & i \\ -i & 1 \end{pmatrix} + \frac{n^{-1/6}}{2(b-a)} \left(\frac{b-a}{z} \right)^{\frac{3}{4}} \begin{pmatrix} 1 & -i \\ i & 1 \end{pmatrix} + \mathcal{O}(n^{-\frac{1}{2}}). \end{aligned}$$

Letting

$$\bar{N}_{a,n} = n^{1/6} \begin{pmatrix} 1 & -i \\ i & 1 \end{pmatrix} + n^{-1/6} \begin{pmatrix} 1 & i \\ -i & 1 \end{pmatrix}$$

we observe that

$$N(a + zn^{-2/3})\bar{N}_{a,n}^{-1} \quad \text{and} \quad \bar{N}_{a,n}N(a + zn^{-2/3})^{-1}$$

are uniformly bounded for z restricted to an annulus around zero as $n \rightarrow \infty$.

We thus remove the growth in the jumps by conjugating: let

$$\Phi_1 = \bar{N}_{a,n}Q_1\bar{N}_{a,n}^{-1}$$

outside O_a (i.e., the simply connected region surrounding a) and

$$\Phi_1 = \bar{N}_{a,n}Q_1$$

inside O_a . The jumps on ∂O_a thus become:

$$Q_1^+ = \bar{N}_{a,n}^{-1} \Phi_1^+ = \bar{N}_{a,n}^{-1} \Phi_1^- G = Q_1^- G \bar{N}_{a,n}$$

and, on the rest of Ω_n^2 ,

$$Q_1^+ = \bar{N}_{a,n}^{-1} \Phi_1^+ \bar{N}_{a,n} = \bar{N}_{a,n}^{-1} \Phi_1^- G \bar{N}_{a,n} = Q_1^- \bar{N}_{a,n}^{-1} G \bar{N}_{a,n},$$

so that Q_1 has bounded jumps.

Once Q_1 and thence Φ_1 are calculated, we need to bound the jump of Φ_2 , which is

$$\Phi_1 G \Phi_1^{-1}.$$

Similar to before, we can find the two-term expansion of $N(b+zn^{-2/3})$ to find $\bar{N}_{b,n}$ to perform a second conjugation. The asymptotic convergence of Φ_1 to I near b ensures that $\bar{N}_{b,n}$ and Φ_1 asymptotically commute.

We can now appeal to Theorem 3 to show asymptotic stability. The boundedness of the jumps can be verified directly. To bound the inverse operators, we can use the boundedness of the parametrix of Section 5.2 when the potential is non-degenerate. In the degenerate case, we would need to use the analysis of the RH problem in [4]. We omit the details here for brevity.

6 Conclusion

We presented a numerical method for computing statistics of unitary invariant ensembles, based on solving the associated Riemann–Hilbert problem numerically. This required solving a nonlinear scalar Riemann–Hilbert problem to calculate the g function associated with the equilibrium measure. Scaling the contours appropriately resulted in a numerical method that remains accurate for large n , without knowledge of the local parametrices.

Our hope is that this framework will lead to a better understanding of the relationship between the potential V , universality laws and finite n statistics.

A Computing a Hastings–McLeod Solution of the Painlevé II transcendent

Here we focus on the (homogeneous) Painlevé II ODE, it is as follows:

$$u''(x) = xu(x) + 2u^3(x). \tag{8}$$

(For brevity we refer to the homogeneous Painlevé II simply as Painlevé II.) There are many important applications of this equation: the Tracy–Widom distribution [27] from random matrix theory is written in terms of the Hastings–McLeod solution [16] and asymptotic solutions to the Korteweg–de Vries and modified Korteweg–de Vries equations can be written in terms of Ablowitz–Segur solutions [1]. The aim of this section is to demonstrate that the RH formulation can indeed be used effectively to compute solutions to Painlevé II, even in the asymptotic regime.

Solutions to differential equations such as (8) are typically defined by initial conditions: at a point x we are given $u(x)$ and $u'(x)$. In the RH formulation, however, we do not specify initial conditions. Rather, the solution is specified by the *Stokes' constants*; constants s_1, s_2, s_3 which satisfy the following condition:

Assumption 3

$$s_1 - s_2 + s_3 + s_1 s_2 s_3 = 0. \quad (9)$$

We will treat the Stokes' constants as given, as, in many applications they arise naturally whilst initial conditions do not. Given such constants, we denote the associated solution to (8) by

$$P_{\text{II}}(s_1, s_2, s_3; z). \quad (10)$$

P_{II} and its derivative can be viewed as the special function which map Stokes' constants to initial conditions.

At first glance, computing solutions to (8) appears trivial: given initial conditions, simply use one's favorite time-stepping algorithm, or better yet, input it into an ODE toolbox such as MATLAB's `ode45` or MATHEMATICA's `NDSolve`. Unfortunately, several difficulties immediately become apparent. In Figure 13, we plot several solutions to (8) (computed using the approach we are advocating): the Hastings–McLeod solution and perturbations of the Hastings–McLeod solution. Note that the solution is inherently unstable, and small perturbations cause oscillations — which make standard ODE solvers inefficient — and poles — which will completely break such ODE solvers (though this issue can be resolved using the methodology of [14]).

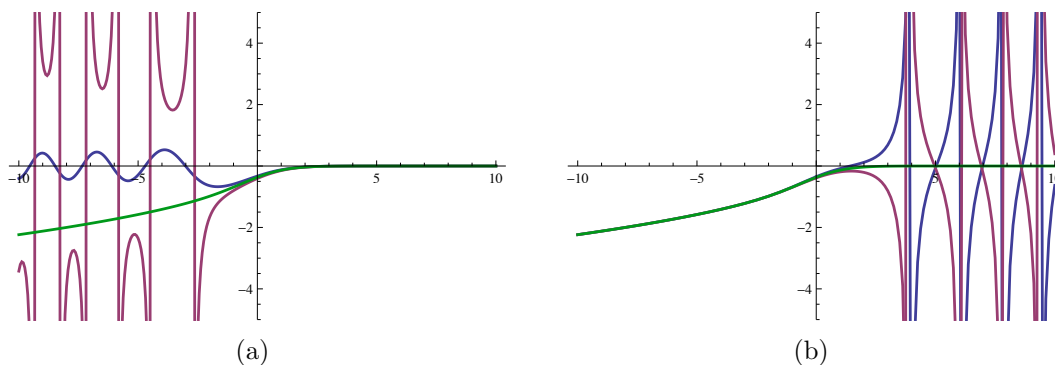


Figure 13: Solutions to Painlevé II. (a) Radically different solutions for $x < 0$. (b) Radically different solutions for $x > 0$.

Remark There are many other methods for computing the Tracy–Widom distribution itself as well as the Hastings–McLeod solution [3, 2], based on the Fredholm determinant formulation or solving a boundary value problem. Moreover, accurate data values have been tabulated using high precision arithmetic with a Taylor series method [24, 25]. However, we will see that there is a whole family of solutions to Painlevé II which exhibit similar sensitivity to initial conditions, and thus a reliable, general numerical method is needed even for this case.

Let $\Phi(x; \lambda)$ solve the RH problem depicted in Figure 14: let $\Gamma = \Gamma_1 \cup \dots \cup \Gamma_6$ for $\Gamma_\kappa \{s e^{i\pi(\kappa/3 - 1/6)} : s \in \mathbb{R}^+\}$, *i.e.*, Γ consists of six rays emanating from the origin, as see in Figure 14. Then the jump matrix is defined by $G(x; \lambda) = G_\kappa(x; \lambda)$ for $z \in \Gamma_\kappa$, where

$$G_\kappa(x; \lambda) = G_\kappa(\lambda) = \begin{cases} \begin{bmatrix} 1 & s_\kappa e^{-i8/3\lambda^3 - 2ix\lambda} \\ & 1 \end{bmatrix} & \text{if } \kappa \text{ even,} \\ \begin{bmatrix} & 1 \\ s_\kappa e^{i8/3\lambda^3 + 2ix\lambda} & 1 \end{bmatrix} & \text{if } \kappa \text{ odd.} \end{cases}$$

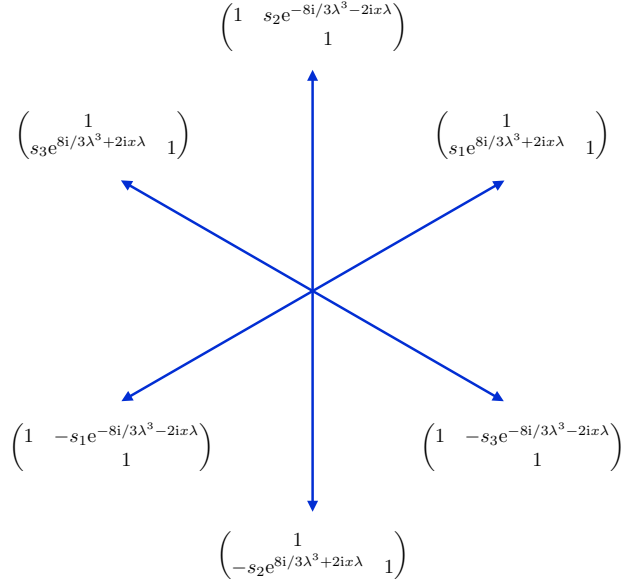


Figure 14: The contour and jump matrix for the Painlevé II RH problem.

This is the RH problem which was solved numerically in [21]. We can recover the corresponding solution to Painlevé II from Φ by [12]

$$P_{\text{II}}(s_1, s_2, s_3; x) = 2 \lim_{\lambda \rightarrow \infty} \lambda \Phi(x; \lambda)_{12}.$$

As $|x|$ becomes large, the jump matrices G are increasingly oscillatory. We will combat this issue by deforming the contour so that these oscillations be exponential decay. To simplify this procedure, we first rescale the RH problem. Note that, if we let $z = \sqrt{|x|}\lambda$, then the jump contour Γ remains unchanged, and

$$\Phi^+(z) = \Phi^+(\sqrt{|x|}\lambda) = \Phi^-(\sqrt{|x|}\lambda)G(\sqrt{|x|}\lambda) = \Phi^-(z)G(z),$$

where $G(z) = G_\kappa(z)$ on Γ_κ for

$$G_\kappa(z) = \begin{cases} \begin{bmatrix} 1 & s_\kappa e^{-i|x|^{3/2}\theta(z)} \\ & 1 \end{bmatrix} & \text{if } \kappa \text{ even,} \\ \begin{bmatrix} & 1 \\ s_\kappa e^{i|x|^{3/2}\theta(z)} & 1 \end{bmatrix} & \text{if } \kappa \text{ odd,} \end{cases}$$

and

$$\theta(z) = \frac{2}{3} (4z^3 + 2e^{i \arg x} z).$$

Then

$$P_{\text{II}}(s_1, s_2, s_3; x) = 2i \lim_{\lambda \rightarrow \infty} \lambda \Phi(x; \lambda)_{12} = 2i\sqrt{x} \lim_{\lambda \rightarrow \infty} z \Phi(x; z)_{12}.$$

A.1 Positive x with $s_1 = 0$

We will now deform the RH problem for Painlevé II so that numerics are asymptotically stable for positive x . We will see that the deformation is extremely simple under the following assumption:

Assumption 4 $s_2 = 0$

We remark that, unlike other deformations, the following deformation can be easily extended to achieve asymptotic stability for x in the complex plane such that $-\frac{\pi}{3} < \arg x < \frac{\pi}{6}$.

On the undeformed contour, the terms $e^{\pm i|x|^{3/2}\theta(z)}$ become oscillatory as $|x|$ becomes large. However, with the right choice of curve $h(t)$, $e^{\pm i\theta(h(t))}$ has no oscillations; instead, it decays exponentially fast as $t \rightarrow \infty$. But h is precisely the path of steepest descent, which passes through the stationary points of θ , *i.e.*, the points where the derivative of θ vanishes. We readily find that

$$\theta'(z) = 2(4z^2 + 1),$$

and the stationary points are $z = \pm i/2$.

We note that, since $G_2 = I$, when we deform Γ_1 and Γ_3 through $i/2$ they become completely disjoint from Γ_4 and Γ_6 , which we then deform through $-i/2$. We also point out that $G_3^{-1} = G_1$ and $G_6^{-1} = G_4$; thus we can reverse the orientation of Γ_3 and Γ_4 , resulting in the jump G_1 on the curve Γ_{\uparrow} and G_4 on Γ_{\downarrow} , as seen in Figure 15.

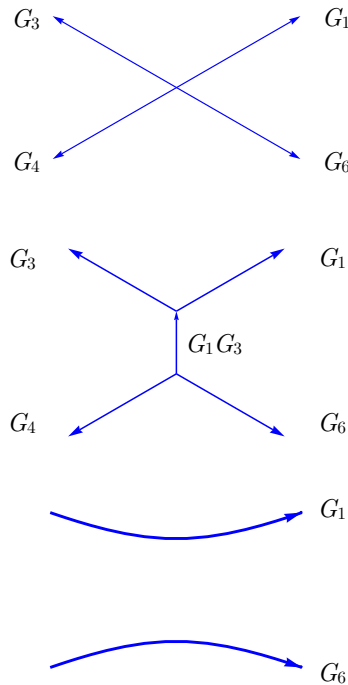


Figure 15: Deforming the RH problem for positive x , with Assumption 4.

Now recall that

$$\theta\left(\pm \frac{i}{2}\right) = \pm \frac{i}{3}.$$

However, we only have Γ_{\uparrow} emanating from $i/2$, with jump matrix

$$G_1 = \begin{bmatrix} 1 & \\ s_1 e^{i|x|^{3/2}\theta(z)} & 1 \end{bmatrix}.$$

This is exponentially decaying to the identity along Γ_{\uparrow} ; as is G_4 along Γ_{\downarrow} . We will employ the approach of Section 5. We first use Lemma 4 to truncate the contours near the stationary

point. What remains is to determine what near means. Because θ behaves like $\mathcal{O}(z \pm i/2)^2$ near the stationary points, Assumption 1 implies that we should choose the shifting of $\beta_1 = i/2$ and $\beta_2 = -i/2$, the scalings $\alpha_1 = \alpha_2 = r|x|^{-3/4}$ and the canonical domains $\Omega_1 = \Omega_2 = [-1, 1]$. Here r is chosen so that what is truncated is negligible in the sense of Lemma 4. G_6 is similar. The complete proof of asymptotic stability of the numerical method proceeds in a similar way as in Section 5.3.1.

A.2 Negative x with $s_1 = -s_3 = \pm i$ and $s_2 = 0$

We now develop deformations for the Hastings–McLeod solution for negative x , which corresponds to $s_1 = \pm i$, $s_2 = 0$ and $s_3 = \mp i$ [12]. We will realize numerical asymptotic stability in the aforementioned sense.

Assumption 5 $s_1 = -s_3 = \pm i$ and $s_2 = 0$

We begin by deforming the RH problem (Figure 14) to the one shown in Figure 16. The horizontal contour extends from $-\alpha$ to α for $\alpha > 0$. We will determine α below. Define

$$G_0 = G_6 G_1 = \begin{bmatrix} s_1 e^{-i|x|^{3/2}\theta(z)} & s_1 e^{-i|x|^{3/2}\theta(z)} \\ s_1 e^{i|x|^{3/2}\theta(z)} & 1 \end{bmatrix}.$$

Note that the assumption $s_2 = 0$ simplifies the form of the RH problem substantially, see Figure 16(b). We use an approach similar to that of the equilibrium measure to replace θ

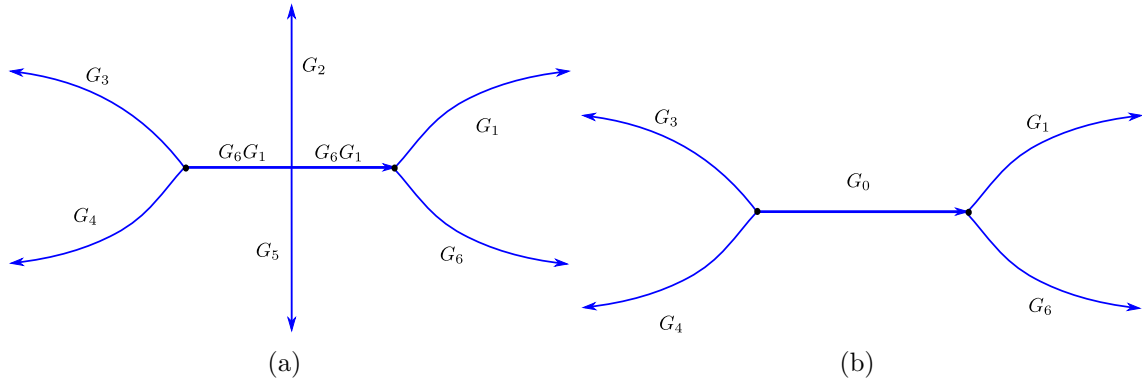


Figure 16: Deforming the RH problem for negative x , with Assumption 5. The black dots represent $\pm\alpha$. (a) Initial deformation. (b) Simplification stemming from Assumption 5.

with a function possessing more desirable properties. Define

$$\Theta(z) = e^{i|x|^{3/2} \frac{g(z) - \theta(z)}{2} \sigma_3}, \quad \sigma_3 = \begin{bmatrix} 1 & \\ & -1 \end{bmatrix}, \quad g(z) = (z^2 - \alpha^2)^{3/2}.$$

The branch cut for $g(z)$ is chosen along $[-\alpha, \alpha]$. If we set $\alpha = 1/\sqrt{2}$ the branch of g can be chosen so that $g(z) - \theta(z) \sim \mathcal{O}(z^{-1})$. Furthermore, $g_+(z) + g_-(z) = 0$ and $\text{Im}(g_-(z) - g_+(z)) > 0$ on $(-\alpha, \alpha)$. Define $\hat{G}_i = \Theta_-^{-1} G_i \Theta_+$ and note that

$$\hat{G}_0(z) = \begin{bmatrix} s_1 e^{-i|x|^{3/2} \frac{g_+(z) + g_-(z)}{2}} & s_1 e^{-i|x|^{3/2} \frac{g_+(z) + g_-(z)}{2}} \\ s_1 e^{i|x|^{3/2} \frac{g_+(z) + g_-(z)}{2}} & e^{i|x|^{3/2} \frac{g_-(z) - g_+(z)}{2}} \end{bmatrix} = \begin{bmatrix} & s_1 \\ s_1 & e^{i|x|^{3/2} \frac{g_-(z) - g_+(z)}{2}} \end{bmatrix}.$$

As $x \rightarrow -\infty$, G_0 tends to the matrix

$$J = \begin{bmatrix} & s_1 \\ s_1 & \end{bmatrix}.$$

The solution of the RH problem

$$\Psi^+(z) = \Psi^-(z)J, \quad z \in [-\alpha, \alpha], \quad \Psi(\infty) = I,$$

is given by

$$\Psi_{\text{HM}}^{\text{out}}(z) = \frac{1}{2} \begin{bmatrix} \beta(z) + \beta(z)^{-1} & -is_1(\beta(z) - \beta(z)^{-1}) \\ -is_1(\beta(z) - \beta(z)^{-1}) & \beta(z) + \beta(z)^{-1} \end{bmatrix}, \quad \beta(z) = \left(\frac{z - \alpha}{z + \alpha} \right)^{1/4}.$$

Here β has a branch cut on $[-\alpha, \alpha]$ and satisfies $\beta(z) \rightarrow 1$ as $z \rightarrow \infty$. It is clear that $(\Psi_{\text{HM}}^{\text{out}})_+ \hat{G}_0 (\Psi_{\text{HM}}^{\text{out}})_-^{-1} \rightarrow I$ uniformly on every closed subinterval of $(-\alpha, \alpha)$.

We define local parametrices near $\pm\alpha$:

$$\Psi_{\text{HM}}^{\alpha} = \begin{cases} I & \text{if } -\frac{\pi}{3} < \arg(z - a) < \frac{\pi}{3} \\ \hat{G}_1^{-1} & \text{if } \frac{\pi}{3} < \arg(z - a) < \pi \\ \hat{G}_1 & \text{if } -\pi < \arg(z - a) < -\frac{\pi}{3} \end{cases},$$

$$\Psi_{\text{HM}}^{-\alpha} = \begin{cases} I & \text{if } \frac{2\pi}{3} < \arg(z + a) < \pi \text{ or } -\pi < \arg(z + a) < -\frac{2\pi}{3} \\ \hat{G}_1^{-1} & \text{if } 0 < \arg(z + a) < \frac{2\pi}{3} \\ \hat{G}_1 & \text{if } -\frac{2\pi}{3} < \arg(z + a) < \frac{2\pi}{3} \end{cases}.$$

We are ready to define the global parametrix. Given $r > 0$ define

$$\Psi_{\text{HM}} = \begin{cases} \Psi_{\text{HM}}^{\alpha} & \text{if } |z - a| < r \\ \Psi_{\text{HM}}^{-\alpha} & \text{if } |z + a| < r \\ \Psi_{\text{HM}}^{\text{out}} & \text{if } |z + a| > r \text{ and } |z - a| > r \end{cases}.$$

It follows that Ψ_{HM} satisfies the RH problem shown in Figure A.2.

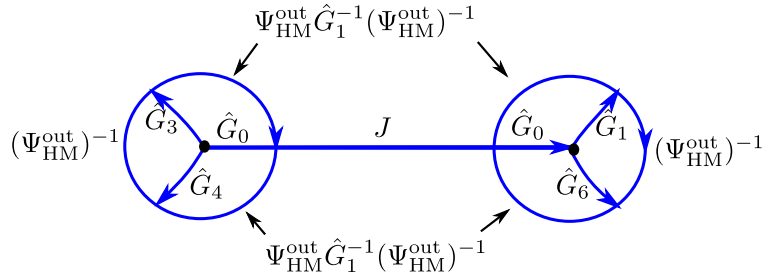


Figure 17: The jump contours and jump matrices for the RH problem solved by Ψ_{HM} . The radius for the two circles is r .

Let Φ be the solution of the RH problem shown in Figure 18(a). It follows that $\Delta = \Phi \Psi_{\text{HM}}^{-1}$ solves the RH problem shown in Figure 18(b). The RH problem for Δ has jump matrices that decay to the identity away from $\pm\alpha$. We use Assumption 1 to determine that we should use $r = |x|^{-1}$. We solve the RH problem for Δ numerically. To compute the solution of Painlevé II we use the formula

$$P_{II}(\pm i, 0, \mp i; x) = 2i \lim_{z \rightarrow \infty} z \Delta(z)_{12}.$$

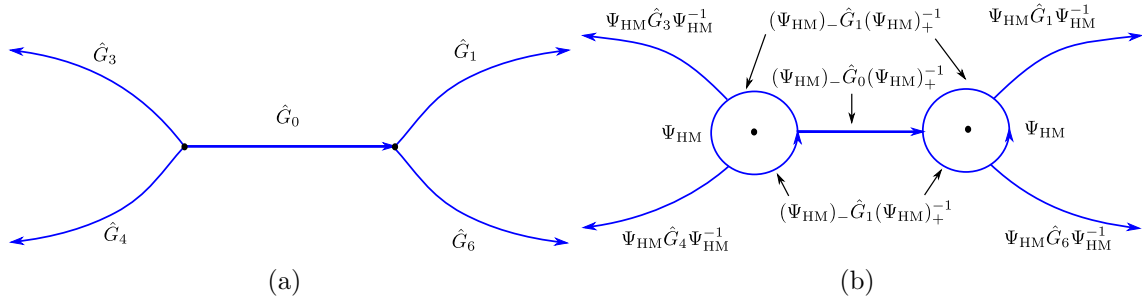


Figure 18: The final deformation of the RH problem for negative x , with Assumption 5. The black dots represent $\pm\alpha$. (a) After conjugation by Θ . (b) Bounding the contours away from the singularities of g and β using Ψ_{HM} .

See Figure 19(a) for a plot of the Hastings–McLeod solution with $s_1 = i$. To verify our computations we may use the asymptotics [12]:

$$P_{\text{II}}(i, 0, -i; x) \sim -\sqrt{\frac{-x}{2}} + \mathcal{O}(x^{-5/2}). \quad (11)$$

We define

$$\left| \frac{P_{\text{II}}(i, 0, -i; x) + \sqrt{\frac{-x}{2}}}{x^{-5/2}} \right|,$$

to be the *relative error* which should tend to a constant for x large and negative. We demonstrate this in Figure 19(b).

Remark Since β has unbounded singularities we expect that a similar issue as in Section 5.3.2 will arise. We do not go through the details of this but this approach produces accurate numerics for all x on the real line.

References

- [1] M. J. Ablowitz and H. Segur. Asymptotic solutions of the Korteweg–de Vries equation. *Stud. in Appl. Math.*, 57:13–44, 1977.
- [2] F. Bornemann. On the numerical evaluation of distributions in random matrix theory. *Markov Process. Related Fields*, 2010.
- [3] F. Bornemann. On the numerical evaluation of Fredholm determinants. *Maths. Comp.*, 79:871–915, 2010.
- [4] T. Claeys, I. Krasovsky, and A. Its. Higher-order analogues of the Tracy–Widom distribution and the Painlevé II hierarchy. *Comm. Pure Appl. Math.*, 63:362–412, 2010.
- [5] T. Claeys and S. Olver. Numerical study of higher order analogues of the Tracy–Widom distribution. *Cont. Maths*, 2011. to appear.
- [6] P. Deift. *Orthogonal Polynomials and Random Matrices: a Riemann–Hilbert Approach*. AMS, 2000.

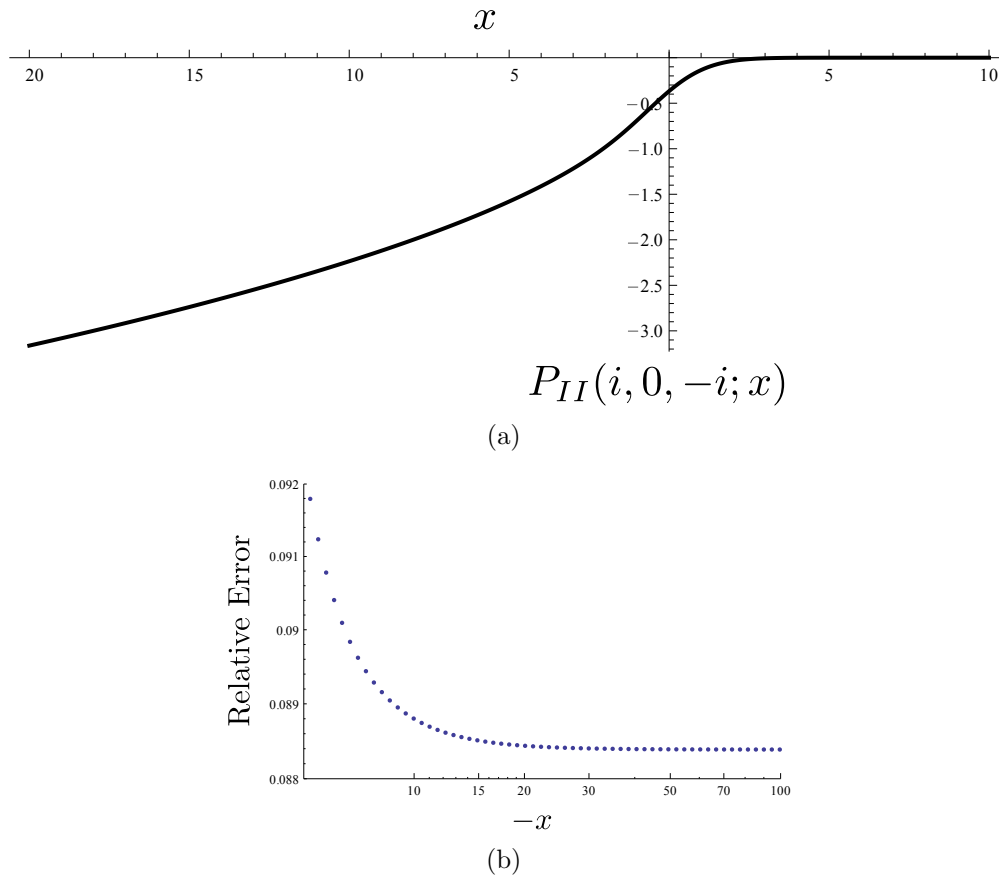


Figure 19: Plotting and analysis of the numerical approximation of $P_{II}(i, 0, -i; x)$. (a) $P_{II}(i, 0, -i; x)$ for positive and negative x . For small $|x|$ we solve the undeformed RH problem. (b) A verification the numerical approximation using the asymptotics (11).

- [7] P. Deift and D. Gioev. Universality at the edge of the spectrum for unitary, orthogonal, and symplectic ensembles of random matrices. *Comm. Pure Appl. Math.*, 60(6):867–910, 2007.
- [8] P. Deift, T. Kriecherbauer, and K. T.-R. McLaughlin. New results on the equilibrium measure for logarithmic potentials in the presence of an external field. *J. Approx. Theory*, 95(3):388–475, 1998.
- [9] P. Deift, T. Kriecherbauer, K. T-R McLaughlin, S. Venakides, and X. Zhou. Asymptotics for polynomials orthogonal with respect to varying exponential weights. *Internat. Math. Res. Notices*, (16):759–782, 1997.
- [10] P. Deift, T. Kriecherbauer, K. T-R McLaughlin, S. Venakides, and X. Zhou. Strong asymptotics of orthogonal polynomials with respect to exponential weights. *Comm. Pure Appl. Math.*, 52(12):1491–1552, 1999.
- [11] P. Deift, T. Kriecherbauer, K. T.-R. McLaughlin, S. Venakides, and X. Zhou. Uniform asymptotics for polynomials orthogonal with respect to varying exponential weights and applications to universality questions in random matrix theory. *Comm. Pure Appl. Math.*, 52(11):1335–1425, 1999.
- [12] A. S. Fokas, A. R. Its, A. A. Kapaev, and V. Y. Novokshenov. *Painlevé Transcendents: the Riemann–Hilbert Approach*. AMS, 2006.

- [13] A. S. Fokas, A. R. Its, and A. V. Kitaev. The isomonodromy approach to matrix models in 2d quantum gravity. *Comm. Math. Phys.*, 147(2):395–430, 1992.
- [14] B. Fornberg and J. A. C. Weideman. A numerical methodology for the Painlevé equations. *J. Comp. Phys.*, 2011.
- [15] W. Gautschi. *Orthogonal Polynomials: Applications and Computation*. Oxford University Press, 2004.
- [16] S. P. Hastings and J. B. McLeod. A boundary value problem associated with the second Painlevé transcendent and the Korteweg–de Vries equation. *Arc. Rat. Mech. Anal.*, 73:31–51, 1980.
- [17] M.L. Mehta. *Random Matrices*. Academic Press, 2004.
- [18] F. W. J. Olver, D. W. Lozier, R. F. Boisvert, and C. W. Clark. *NIST Handbook of Mathematical Functions*. Cambridge University Press, 2010.
- [19] S. Olver. Computation of equilibrium measures. *J. Approx. Theory*, 163:1185–1207, 2011.
- [20] S. Olver. Computing the Hilbert transform and its inverse. *Math. Comp.*, 80:1745–1767, 2011.
- [21] S. Olver. Numerical solution of Riemann–Hilbert problems: Painlevé II. *Found. Comput. Math.*, 11:153–179, 2011.
- [22] S. Olver. A general framework for solving Riemann–Hilbert problems numerically. *Numer. Math.*, 122:305–340, 2012.
- [23] S. Olver and T. Trogdon. Nonlinear steepest descent and the numerical solution of Riemann–Hilbert problems. [arXiv:1205.5604 \[math.NA\]](https://arxiv.org/abs/1205.5604), 2012.
- [24] M. Prähofer and H. Spohn. Exact scaling functions for one-dimensional stationary KPZ growth. <http://www-m5.ma.tum.de/KPZ/>.
- [25] M. Prähofer and H. Spohn. Exact scaling functions for one-dimensional stationary KPZ growth. *J. Stat. Phys.*, 115:255–279, 2004.
- [26] E. B. Saff and V. Totik. *Logarithmic Potentials with External Fields*. Springer, 1997.
- [27] C. A. Tracy and H. Widom. Level-spacing distributions and the Airy kernel. *Comm. Math. Phys.*, 159:151–174, 1994.